Athenea

Revista en Ciencias de la Ingeniería

ISSN: 2737-6439
DOI: 10.47460/athenea
Volume 4, Issue 14
December 2023

Published by:

AutanaBooks
Engineering & Services

ATHENEA JOURNAL

JOURNAL IN ENGINEERING SCIENCES

Electronic Journal Edited By AutanaBooks.

Quarterly Periodicity

Our cover:

Athenea, Engineering Sciences Magazine is pleased to bring a new issue where it continues to support Latin American research.

Volume 4 // Issue 14 // December 2023
DOI:10.47460/athenea
ISSN: 2737-6439

Viewing the Journal:
https://athenea.autanabooks.com/index.php/revista

"by the grace of God"

Publisher: Dr. Franyelit Suárez,
http://orcid.org/0000-0002-8763-5513
editorial@autanabooks.com
AutanaBooks, Quito, Ecuador

DIRECTORY OF THE ATHENEA
JOURNAL IN ENGINEERING SCIENCES

ACADEMIC COMMITTEE

Athenea Journal
Volume 4 // Issue 14 // December 2023
DOI:10.47460/athenea/v4i14
ISSN: 2737-6439

Content

Editorial

In this new issue of Athenea Journal in Engineering Sciences, we take a journey to the deepest corners of the human mind and the wonders that arise from the conjunction of Artificial Intelligence, Technology, and Engineering. In this issue, we delve into the beating heart of innovation, where masterminds challenge the boundaries of the conceivable and lead us into a future imbued with infinite possibilities. Artificial intelligence, like the fire that once gave us light in the darkness, now leads us to unexplored horizons. From algorithms that learn and evolve to systems that interpret emotions, in this issue of our magazine, we will unravel the wonders of AI that transform not only the way we live, but also the very essence of our existence.

In the vast universe of technology, every innovation is a constellation waiting to be discovered. From augmented reality that immerses us in parallel worlds to cybersecurity that protects our most precious secrets, we will address the current technological landscape with an incisive approach. The technological revolution is not only inevitable; It is an invitation to imagine and build the future we want to see. Engineering, like the architect of tangible dreams, guides us in the creation of realities that seemed reserved for science fiction. From projects that defy gravity to sustainable solutions that preserve our planet, we will explore engineering as the driving force behind a rapidly evolving world.

This issue is not just a collection of articles; is a testament to the inquiring minds that challenge the norm and build bridges to the future. From the creative minds who conceive new realities to the engineers who bring those visions to life, we celebrate those who, with every line of code and every designed structure, are writing the next chapter in human history. In this way, Athenea Journal publishes the results of research that is born from the passion for engineering, science and technology, to contribute to an increasingly challenging world and society.

Dr. Franyelit Suárez

ISSN-e: 2737-6419

Athenea Journal
Vol.4, Issue 14, (pp. 8-21)

https://doi.org/10.47460/athenea.v4i14.64

Algorithm for Diffuse TSK Modeling of SNL MIMO with Undefined Operation Points

Luis J. Gonzalez Lugo
https://orcid.org/0000-0001-9933-4147
lgonzalez@ingenieriala.com
LA Engineering
Frutillar-Chile

Received (22/09/2023), Accepted (10/11/2023)

Abstract. - This paper presents an algorithm for constructing fuzzy models in linear state subspaces from the nonlinear MIMO dynamic model of plants whose operating points are not defined within the permissible physical range for the system. It is based on the fuzzy Takagi-Sugeno-Kang model and Kawamoto's ideas of non-linearity sectors. The relevant functions in the antecedent are modeled with linear functions, while functions model the consequent in Discrete State Space. The application of the algorithm to the model of a thermoelectric plant widely studied in the specialized literature is discussed.

Keywords: Fuzzy modeling algorithm, undefined points of operation, Kawamoto non-linearity sectors, nonlinear MIMO systems, Takagi-Sugeno-Kang.

Algoritmo para el modelado TSK difuso de SNL MIMO con puntos de operación indefinidos

Resumen: En este artículo se presenta un algoritmo para la construcción de modelos difusos en subespacios de estado lineales a partir del modelo dinámico MIMO no lineal de plantas cuyos puntos de operación – dentro del rango físico permisible para el sistema – no se encuentran definidos. Se toma como base el modelo difuso Takagi-Sugeno-Kang y las ideas de sectores de no linealidad de Kawamoto. Las funciones de pertinencia en el antecedente se modelan con funciones lineales, en tanto que el consecuente se modela mediante funciones en Espacio de Estado Discreto. Se discute la aplicación del algoritmo al modelo de una planta termoeléctrica ampliamente estudiada en la literatura especializada.

Palabras clave: Algoritmo modelado difuso, puntos de operación indefinidos, sectores de no-linealidad Kawamoto, sistemas MIMO no-lineales, Takagi-Sugeno-Kang.

I. INTRODUCTION

To control means to exert the actions necessary to produce a desired result, but to do so, the system to be commanded must exhibit "reasonably predictable" behavior. In the specialized literature [1], it is proposed that the systems to be controlled can be classified into two large groups: deterministic and non-deterministic. Classical control algorithms are based on the hypothesis that the system to be controlled is deterministic, for which a series of restrictions are applied to guarantee the functionality of the algorithm, ranging from restricting the work area to a small region around a point of operation, to "disregarding" the probabilistic nature of the present and future state of the system. There is also a presumption that the mathematical model of the system is time-invariant. However, these classical control techniques work very well for various physical systems and have been successfully employed for over a century, as stated in [2]: "Most physical systems contain complex non-linear relationships, which are difficult to model with conventional techniques." That is why, in advanced process control, non-linear control techniques are used.

One of the ways to mathematically model the non-linear nature of systems is by using models based on fuzzy logic systems. This theory is supported by fuzzy logic systems being universal approximators [2]. In particular, the fuzzy system model developed by Takagi and Sugeno [3] and Sugeno and Kang [4], called the TSK fuzzy model in the literature, is suitable for a broad class of non-linear systems because the consequent is a linear function or even a state-space system. Interestingly, the TSK model allows the use of equations in State Spaces in the consequent, thus being able to obtain a fuzzy model for a Non-linear System (SNL) of multiple inputs and outputs (MIMO), which allows the application of modern control algorithms based on models in State Space such as Optimal Control, H∞, Genetic Algorithms, Predictive Control.

The fuzzy model of an SNL MIMO is robust in applications where the plant has more than one operating point. However, following conventional techniques, as the number of operation points increases, the fuzzy model increases significantly in complexity since, in general, a linear subspace is generated for each operation point, that is, a rule in the consequent. It has also been sufficiently studied that as the number of rules in the consequent increases, the fuzzy TSK model exhibits a behavior closer and closer to the non-linear model of the system. Thus, there is a dilemma between keeping the complexity of the fuzzy model low – few rules – and, at the same time, ensuring that it represents the dynamics of the SNL as accurately as possible.

Now, imagine for a moment that a TSK model is required for an SNL MIMO whose operating points – within the permissible physical range for the system – are not defined, as might be the case with the design of a fuzzy servo controller for such a system. Undoubtedly, this last proposition introduces an additional level of complexity to the previously posed dilemma between keeping the number of rules of the fuzzy model to a minimum and, at the same time, representing the system as accurately as possible, the complexity of not having defined the points of operation. Next, an algorithm is presented to solve the problem: synthesize the fuzzy TSK model of a MIMO SNL with undefined operation points.

II. DEVELOPMENT

In the first instance, a synthesis of the theoretical foundations of the developed algorithm is presented, and then a detailed description is given.

A. Takagi-Sugeno-Kang Fuzzy Model (TSK)

Takagi and Sugeno [3], and later Sugeno and Kang [4], developed the structure of a Fuzzy Model that has been widely studied. They denoted the relevance function of a fuzzy set A as *A(x),* with x $\in$ *X,* and defined that all fuzzy sets are associated with linear relevance functions, such that a relevance function is characterized by having two limit values: 1 for the highest degree of relevance and 0 for the lowest degree of significance. Thus, the *Truth Value* of a linguistic proposition of the type "(x is A) Y (y is B)" is expressed as:

$$|"(x\ is\ A)\ and\ (y\ is\ B)"| = A(x) \wedge B(y) \qquad (1)$$

In addition, these researchers defined the format of a fuzzy R implication as:

$$R: If\ f(x_1\ is\ A_1, \ldots, x_k\ is\ A_k), Then\ y = g(x_1, \ldots, x_k) \qquad (2)$$

Where:

y	:	a variable of the consequent whose value is inferred.
$x_1 - x_k$	:	premise variables that also appear in the consequent.
$A_1 - A_k$	:	fuzzy sets with linear relevance functions representing a subspace in which the implication R can be applied by reasoning.
f	:	logical function that relates the propositions in the antecedent.
G	:	a function that involves the value of "y" in the consequent when $x_1 - x_k$ satisfies the antecedent.

If only logical functions are used in the antecedent, and a linear function is adopted in the consequent, implication (2) is written as:

$$R: If\ f(x_1\ is\ A_1\ and \dots\ and\ x_k\ is\ A_k) \\ Then\ y = p_0\ +\ p_1x_1 + \dots\ + p_kx_k \quad (3)$$

In addition, if i have implications R_i $(i = 1, \cdots, n)$ according to the format indicated in (3). When given:

$$\left(x_1 = x_{10}, \cdots, x_k = x_{k0}\right) \quad (4)$$

where x_{10} - x_{k0} are singletons, the value of y is inferred using the following algorithm:

1) For each implication Ri, y^i is computed by the function g_i of the consequent:

$$y^i = p_0^i + p_1^i x_1^0 + \cdots + p_k^i x_k^0 \quad (5)$$

2) The Truth Value of the proposition y = y^i is calculated by the equation:

$$\left|y = y^i\right| = \left(A_1^i\left(x_{10}\right) \wedge \cdots \wedge A_k^i\left(x_{k0}\right)\right) \quad (6)$$

Where $|*|$ denotes the Truth Value of the proposition, represents the minimum operation, and $\wedge$ A(x_0) is the degree of pertinence of x_0 to the fuzzy set A.

3) Finally, the value of y is inferred from the n implications as its weighted average such that:

$$y = \frac{\sum_{i=1}^{n}\left[\left|y = y^i\right| \times y^i\right]}{\left|y = y^i\right|} \quad (7)$$

B. Kawamoto's Non-Linearity Sectors

According to Mehran [5], the idea of using Non-Linearity Sectors in the construction of fuzzy models was first proposed by Kawamoto [6]. Consider an SNL such that:

$$\dot{x} = f\left(x(t)\right) \quad (8)$$

Where $f(0) = 0$. The aim is to define the global sector in such a way that:

$$\dot{x} = f\left(x(t)\right) \in \left[a_1, a_2\right] x(t) \quad (9)$$

Figure 1 illustrates the nonlinearity sector approach.

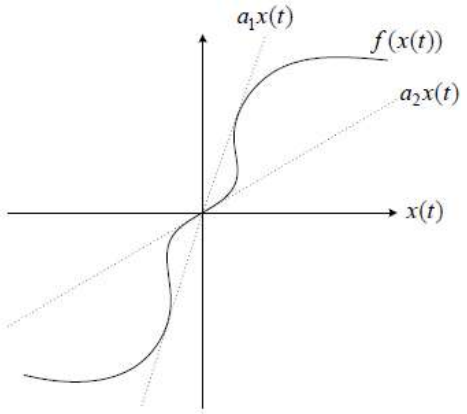

Figure 1. Non-Linearity Sectors.

C. Algorithm for Constructing the TSK Model of a MIMO SNL with Undefined Points of Operation.

Mehran [5] argues that, although the consequent variables can be continuous or discrete in theory, they must be discrete because virtually all fuzzy systems are implemented and modeled using digital systems. Based on the ideas of Takagi, Sugeno, Kawamoto, and Mehran, the following algorithm was designed for the TSK modeling of a MIMO SNL whose operation points are undefined.

Algorithm:

1) From the differential equations of the MIMO SNL, algebraically determine the state-space model for the SNL by considering a generic operation point **(X_0, U_0)**. Such that:

$$\begin{aligned}\dot{\bar{X}}(n+1) &= A(X_0,U_0)\bar{X}(n) + B(X_0,U_0)\bar{U}(n)\\ \bar{Y}(n) &= C(X_0,U_0)\bar{X}(n) + D(X_0,U_0)\bar{U}(n)\end{aligned} \quad (10)$$

2) Analyze the Jacobian matrices *A,* B, *C*, and *D* to determine which variables they depend on. These will be the k premise variables of the TSK model.

3) Analyze the maximum and minimum allowable physical values for the premise variables according to the characteristics of the SNL, or what the maximum and minimum values are for which the SNL model in differential equations is valid. From these, some steady-state pseudo-points of operation of the SNL MIMO are defined and used to obtain the relevance functions of the antecedent and the Jacobian matrices of the consequent. For pseudo-points of operation, the following must be met:

$$0 = A\left(X_0,U_0\right)\bar{X} + B\left(X_0,U_0\right)\bar{U} \quad (11)$$

4) Define the linear relevance functions based on the previous step's results.

5) Define the $n=2^k$ implications of the TSK model according to the following structure:

$$\begin{aligned}&R^i: if(z_1\ is\ A_1\ and \cdots and\ z_k is A_k)\\ Then\{\ &\dot{\bar{X}}(n+1) = A(X_0,U_0)\bar{X}(n) + B(X_0,U_0)\bar{U}(n)\\ &\bar{Y}(n) = C(X_0,U_0)\bar{X}(n) + D(X_0,U_0)\bar{U}(n)\end{aligned} \quad (12)$$

6) Infer the value of the output vector from (6) and (7).

III. ALGORITHM AND APPLICATION STUDY

To illustrate the application of the presented algorithm and to verify its effectiveness, the comparison of the results obtained in the modeling of a Thermoelectric Plant widely worked in the specialized literature [7], [8], [9], [10], [11], using both the traditional algorithm based on operating points and the algorithm developed in the research carried out will be presented as a case study.

A. SNL MIMO: Thermoelectric Plant

The model is based on the P16/G16 Thermoelectric Plant at the Sydvenska Kraft AB Plant in Malmö, Switzerland. The power of the Plant is 160 MW, with a Boiler-Turbine-Alternator structure. The 3rd-order model of this SNL MIMO was developed by Bell and Aström [12]. The differential equations that define the dynamics of this MIMO SNL are presented in (13) , (14) and (15):

$$\dot{p} = -0,0018u_2 p^{9/8} + 0,9u_1 - 0,15u_3 \quad (13)$$

$$\dot{P}_o = (0,073u_2 - 0,016)p^{9/8} - 0,1P_o \quad (14)$$

$$\dot{\rho}_f = \frac{\left(141u_3 - \left(1,1u_2 - 0,19\right)p\right)}{85} \quad (15)$$

Where p is the Pressure in the boiler [kg/cm^2], P_o is the electrical power generated [MW], ρ_f is the density of the fluid [kg/m^3], u_1 is the position of the fuel flow valve, u_2 is the position of the steam control valve, and u_3 is the position of the water flow valve. All u_i inputs are normalized in the range [0,1]. Without losing generality, the system outputs are considered the state variables for this study case.

Dimeo and Lee [7] presented the seven points of operation of the Thermoelectric Plant under study, reproduced in Table 1.

Table 1. Thermoelectric Plant Operation Points.

	1	2	3	4	5	6	7
p_0	75,60	86,40	97,20	108,0	118,8	129,6	140,4
P_{o0}	15,27	36,65	50,52	66,65	85,06	105,8	128,9
ρ_{f0}	299,6	342,4	385,2	428,0	470,8	513,6	556,4
u_{10}	0,156	0,209	0,271	0,340	0,418	0,505	0,600
u_{20}	0,483	0,552	0,621	0,690	0,759	0,828	0,897
u_{30}	0,183	0,256	0,340	0,435	0,543	0,663	0,793

B. Discrete TSK Model Based on Points of Operation

To construct the Discrete TSK model Based on the Operating Points of the thermoelectric plant, in the first instance, seven linear subspaces are defined – one for each point of operation indicated in Table 1, then the triangular relevance functions for each of the state variables are described in the antecedent as shown in Figures 2, 3 and 4. Thus, for a given linear subspace, the Truth Value of the proposition, according to (6), is provided by the expression:

$$\left|X = X^i\right| = \left(A_1^i\left(x_{1_0}\right) \wedge A_2^i\left(x_{2_0}\right) \wedge A_3^i\left(x_{3_0}\right)\right) \quad (16)$$

In the case of the consequent, we work with discrete state space models around each point of operation presented in Table 1. Linearized models are obtained from the truncated Taylor series expansion of the SNL represented by the equations(13), (14) and (15). To do this, it is necessary to calculate the following Jacobian matrices:

$$A = \left.\frac{\delta F}{\delta X}\right|_{(X_0, U_0)} \quad (17)$$

$$B = \left.\frac{\delta F}{\delta U}\right|_{(X_0, U_0)} \quad (18)$$

So, the linear approximation of the system will be:

$$\dot{\bar{X}} = A\bar{X} + B\bar{U} \quad (19)$$

where:

$$\bar{X} = X - X^0, X = \left[p\ P_o\ \rho_f\right]^T = \left[x_1\ x_2\ x_3\right]^T \quad (20)$$

$$\bar{U} = U - U^0, U = \left[u_1\ u_2\ u_3\right]^T \quad (21)$$

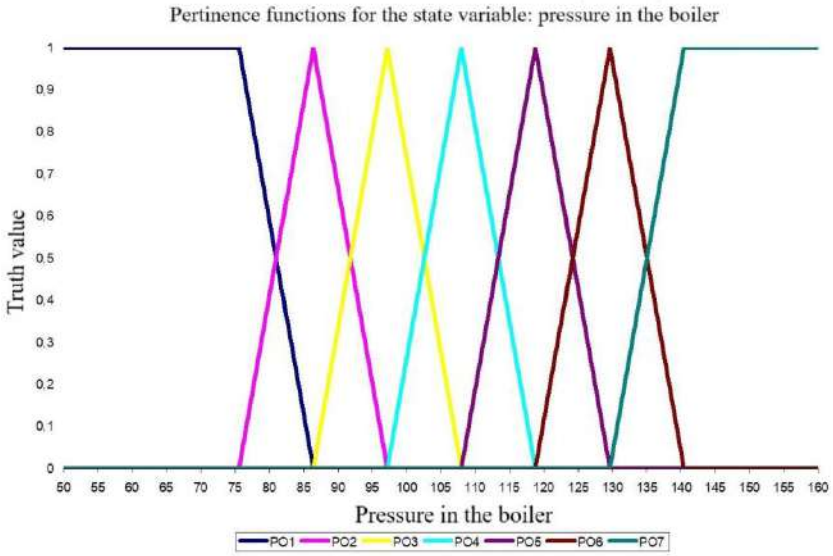

Figure 2. Relevance Functions of the Traditional Discrete TSK Model for Boiler Pressure.

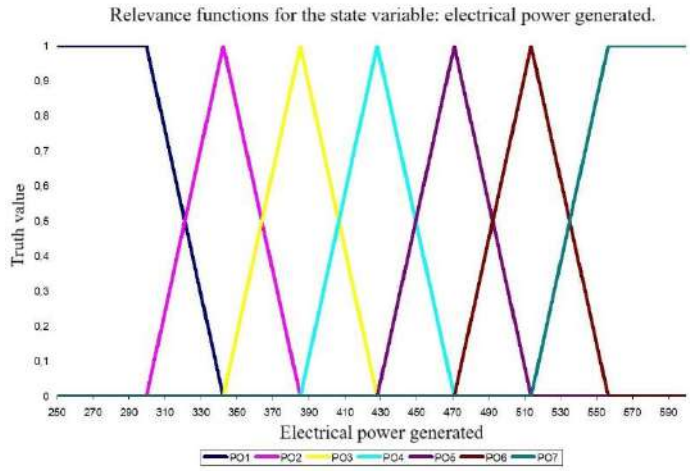

Figure 3. Relevance Functions of the Traditional Discrete TSK Model for Generated Electrical Power.

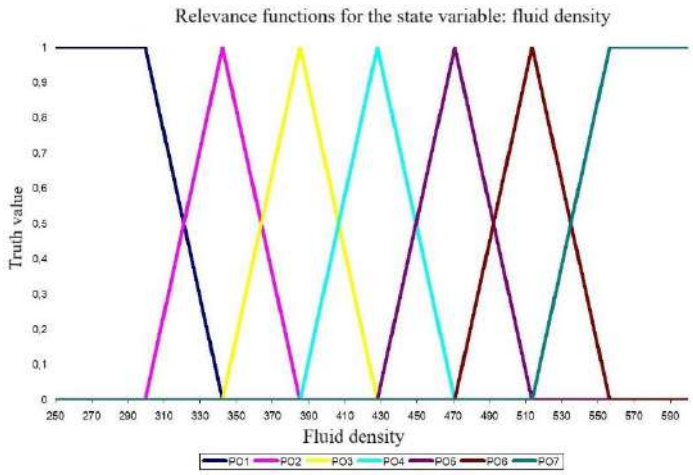

Figure 4. Relevance Functions of the Traditional Discrete TSK Model for Fluid Density.

It was subsequently, using a zero-order retainer-type conversion algorithm, with a sampling time of 60 seconds, the seven pairs of matrices presented from (22) to (28).

$$A_d^1=\begin{bmatrix}0,9355 & 0 & 0\\ 0,1416 & 0,0025 & 0\\ -0,1172 & 0 & 1,0000\end{bmatrix}, B_d^1=\begin{bmatrix}73,1364 & -14,6469 & -12,1894\\ 9,1908 & 100,2430 & -1,5318\\ -4,4779 & -64,3485 & 140,0875\end{bmatrix} \quad (22)$$

$$A_d^2=\begin{bmatrix}0,9237 & 0 & 0\\ 0,2121 & 0,0025 & 0\\ -0,1549 & 0 & 1,0000\end{bmatrix}, B_d^2=\begin{bmatrix}73,6787 & -18,8617 & -12,1131\\ 13,8405 & 128,6948 & -2,3067\\ -5,9344 & -80,6090 & 140,3303\end{bmatrix} \quad (23)$$

$$A_d^3=\begin{bmatrix}0,8895 & 0 & 0\\ 0,4317 & 0,0025 & 0\\ -0,2779 & 0 & 1,0000\end{bmatrix}, B_d^3=\begin{bmatrix}71,3414 & -21,5197 & -11,8902\\ 28,6071 & 145,1289 & -4,7678\\ -10,7098 & -90,6696 & 141,1262\end{bmatrix} \quad (24)$$

$$A_d^4=\begin{bmatrix}0,8749 & 0 & 0\\ 0,5217 & 0,0025 & 0\\ -0,3258 & 0 & 1,0000\end{bmatrix}, B_d^4=\begin{bmatrix}70,7640 & -24,3791 & -11,7940\\ 34,8055 & 163,6185 & -5,8009\\ -12,5898 & -101,3357 & 141,4395\end{bmatrix} \quad (25)$$

$$A_d^5=\begin{bmatrix}0,8603 & 0 & 0\\ 0,6108 & 0,0025 & 0\\ -0,3729 & 0 & 1,0000\end{bmatrix}, B_d^5=\begin{bmatrix}70,1853 & -27,2193 & -11,6975\\ 41,0290 & 181,7735 & -6,8382\\ -14,4483 & -111,7990 & 141,7493\end{bmatrix} \quad (26)$$

$$A_d^6=\begin{bmatrix}0,8457 & 0 & 0\\ 0,6988 & 0,0025 & 0\\ -0,4191 & 0 & 1,0000\end{bmatrix}, B_d^6=\begin{bmatrix}69,6057 & -30,0499 & -11,6009\\ 47,2645 & 199,6554 & -7,8774\\ -16,2853 & -122,1120 & 142,0554\end{bmatrix} \quad (27)$$

$$A_d^7=\begin{bmatrix}0,8313 & 0 & 0\\ 0,7854 & 0,0025 & 0\\ -0,4646 & 0 & 1,0000\end{bmatrix}, B_d^7=\begin{bmatrix}69,0260 & -32,8642 & -11,5043\\ 53,4991 & 217,2193 & -8,9165\\ -18,1007 & -132,2649 & 142,3580\end{bmatrix} \quad (28)$$

Finally, the defusification is performed using the equations (6) and (7).

C. TSK Discrete Model for Undefined Points of Operation

The following is the development of the proposed algorithm to obtain the TSK Discrete model of the thermoelectric plant.

1) The differential equations of the SNL MIMO presented in (13), (14) and (15), are linearized using (17) and (18) around a generic point of operation (X_0, U_0), yielding:

$$\dot{\bar{X}} = A(X_0,U_0)\,\bar{X} + B(X_0,U_0)\bar{U} \quad (29)$$

$$A(X_0,U_0)=\begin{bmatrix}-0,002025u_{2_0}\left(x_{1_0}\right)^{1/8} & 0 & 0\\ \left(0,082125u_{2_0}-0,018\right)\left(x_{1_0}\right)^{1/8} & -0,1 & 0\\ -0,01294118u_{2_0}+0,002235294 & 0 & 0\end{bmatrix} \quad (30)$$

$$B(X_0,U_0)=\begin{bmatrix}0,9 & -0,0018\left(x_{1_0}\right)^{9/8} & -0,15\\ 0 & 0,073\left(x_{1_0}\right)^{9/8} & 0\\ 0 & -0,01294118x_{1_0} & 1,658824\end{bmatrix} \quad (31)$$

2) Analyzing (30) and (31), it is concluded that the Jacobian matrices of the linearized system only depend on the variables x_1 and U_2, so these become the premise variables of the TSK model (*k=2).*

3) By analyzing the maximum and minimum physical values of the premise variables x_1 and U_2 and considering that the condition is met (11), the pseudo-points of operation presented in Table 2 are obtained.

Table 2. Pseudo-Operation Points of the Thermoelectric plant.

	T_o	B	c	d
x_{10}	60,02	60,02	165,00	165,00
x_{20}	8,03	51,32	25,02	159,90
x_{30}	275,00	165,80	462,30	474,20
u_{10}	0,0780	0,2427	0,2388	0,7358
u_{20}	0,3287	0,9208	0,3287	0,9208
u_{30}	0,0730	0,3502	0,2008	0,9630

From Table 2, note that for x_1 (Pressure), 60.02 [kgf/cm^2] and 165.00 [kgf/cm^2] have been defined as the minimum and maximum values, respectively, for this premise variable, while for the position of the steam control valve, U_2 0.3287 and 0.9208 have been defined as their maximum and minimum values; from these and from (11), (13), (14) and (15), the rest of the data contained in Table 2 were obtained.

4) Based on the results presented in Table 2, the relevance functions shown in Figures 5 and 6 are defined.

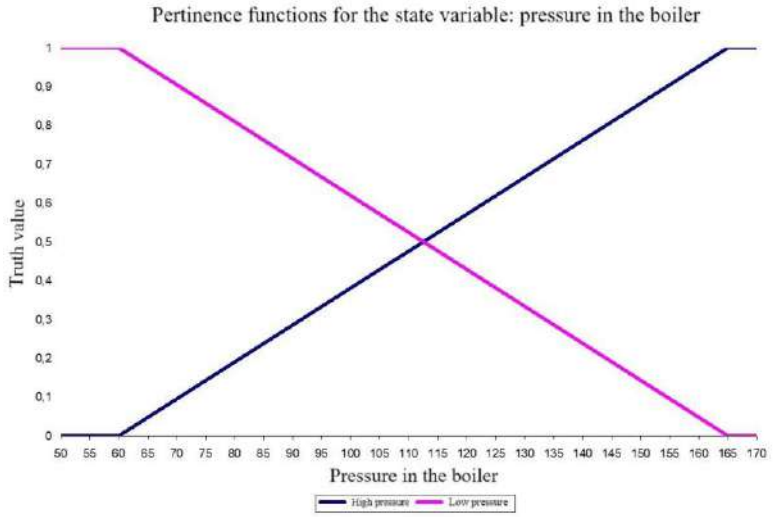

Figure 5. Relevance Functions of the Proposed Discrete TSK Model for Boiler Pressure.

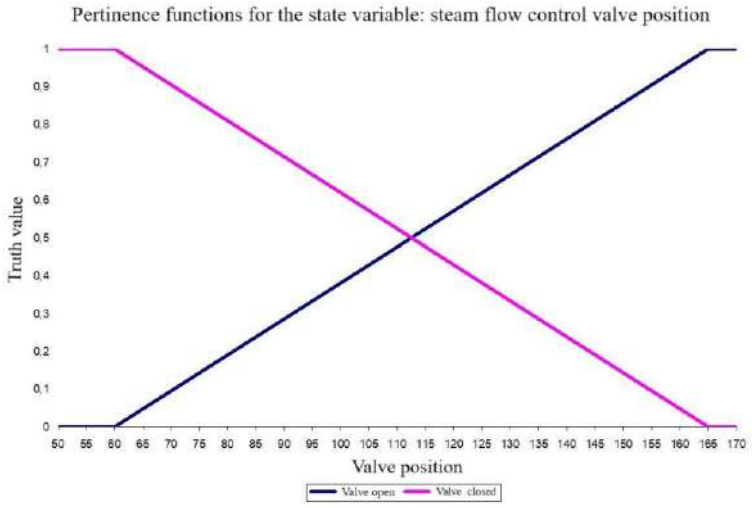

Figure 6. Relevance Functions of the Proposed Discrete TSK Model for Steam Control Valve Position.

Figure 6. Relevance Functions of the Proposed Discrete TSK Model for Steam Control Valve Position.

5) The n=22 implications of the Discrete TSK model is defined:

$$R_1: if(x_1 \text{ is "low"} \wedge u_2 \text{ is "closed"})$$
$$Then: \bar{X}_1(n+1) = A_1\bar{X}_1(n) + B_1\bar{U}_1(n) \quad (32)$$

Where:

$$A_1 = \begin{bmatrix} 0,9355 & 0 & 0 \\ 0,1416 & 0,0025 & 0 \\ -0,1172 & 0 & 1,0000 \end{bmatrix}, B_1 = \begin{bmatrix} 73,1364 & -14,6469 & -12,1894 \\ 9,1908 & 100,2430 & -1,5318 \\ -4,4779 & -64,3485 & 140,0875 \end{bmatrix} \quad (33)$$

$$R_2: if(x_1 is \text{ "low"} \wedge u_2 \text{ is "opened"})$$
$$Then: \bar{X}_2(n+1) = A_2\bar{X}_2(n) + B_2\bar{U}_2(n) \quad (34)$$

Where:

$$A_2 = \begin{bmatrix} 0,8297 & 0 & 0 \\ 0,8208 & 0,0025 & 0 \\ -0,5299 & 0 & 1,0000 \end{bmatrix}, B_2 = \begin{bmatrix} 68,9638 & -13,8113 & -11,4940 \\ 55,9540 & 90,8778 & -9,3257 \\ -20,6518 & -61,1094 & 142,7832 \end{bmatrix} \quad (35)$$

$$R_3: if(x_1 is \text{ "high"} \wedge u_2 \text{ is "closed"})$$
$$Then: \bar{X}_3(n+1) = A_3\bar{X}_3(n) + B_3\bar{U}_3(n) \quad (36)$$

Where:

$$A_3 = \begin{bmatrix} 0,9272 & 0 & 0 \\ 0,1595 & 0,0025 & 0 \\ -0,1166 & 0 & 1,0000 \end{bmatrix}, B_3 = \begin{bmatrix} 72,8127 & -45,4890 & -12,1355 \\ 10,3892 & 311,9603 & -1,7315 \\ -4,4647 & -176,5755 & 140,0853 \end{bmatrix} \quad (37)$$

$$R_4: if(x_1 is \text{ "high"} \wedge u_2 \text{ is "opened"})$$
$$Then: \bar{X}_4(n+1) = A_4\bar{X}_4(n) + B_4\bar{U}_4(n) \quad (38)$$

Where:

$$A_4 = \begin{bmatrix} 0,8091 & 0 & 0 \\ 0,9121 & 0,0025 & 0 \\ -0,5235 & 0 & 1,0000 \end{bmatrix}, B_4 = \begin{bmatrix} 68,1305 & -42,5638 & -11,3551 \\ 62,8271 & 279,2003 & -10,4712 \\ -20,4850 & -166,5670 & 142,7554 \end{bmatrix} \quad (39)$$

In general:

$$\bar{X}_i(n) = X(n) - X_{i_0}, \ \bar{U}_i(n) = U(n) - U_{i_0} \quad (40)$$

7) The value of the output is inferred from (6) and (7).

IV. RESULTS

Two comparative studies were conducted to show the performance of the Discrete TSK model developed with the proposed algorithm. The first study consisted of subjecting the three models (the non-linear, the Fuzzy model with seven rules, and the Fuzzy model formulated with the proposed algorithm) to a sequence of ascending and descending inputs according to the seven points of operation presented in Table 1. The second comparative study involved subjecting the three models to a pseudo-random sequence of the three input variables, respecting the established limits (minimum and maximum values) for each input in Table 1.

For both comparative studies, Variation Accounting (VAF) and Mean Square Error (RMSE) were considered as performance indices, indices used by Castillo, Sarmiento, and Sanz [13] when performing the comparative evaluation of a similar discrete TSK model. Recall that as two signals in a time series are almost identical, the RMSE tends to zero, while the VAF tends to 100%.

Figures 7 to 10 present the most relevant results of the first comparative study, while Figures 11 to 14 present the results of the second study.

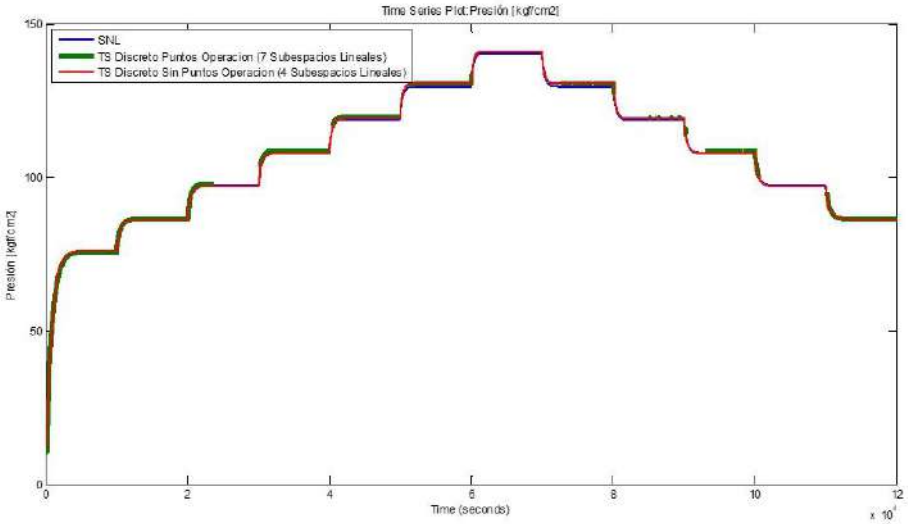

Figure 7. Comparison of the estimation of the Pressure in the Boiler of the Thermoelectric Plant for case 1.

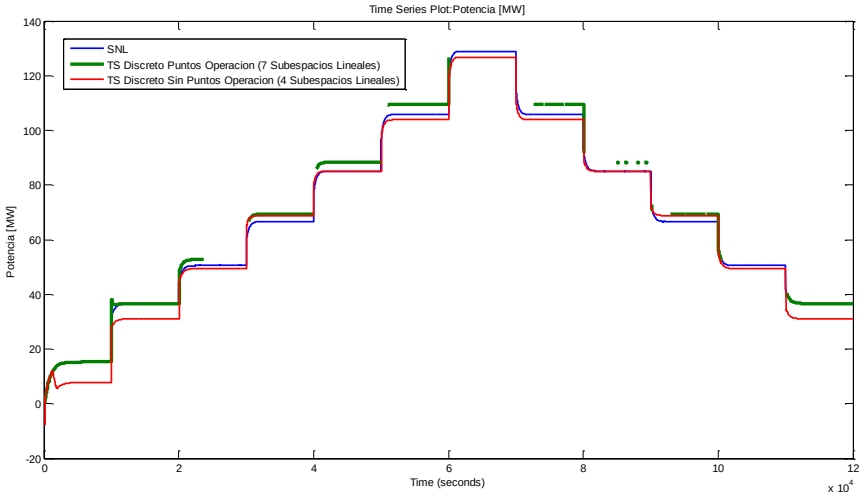

Figure 8. Comparison of the estimation of the Power Output of the Thermoelectric Plant for case 1.

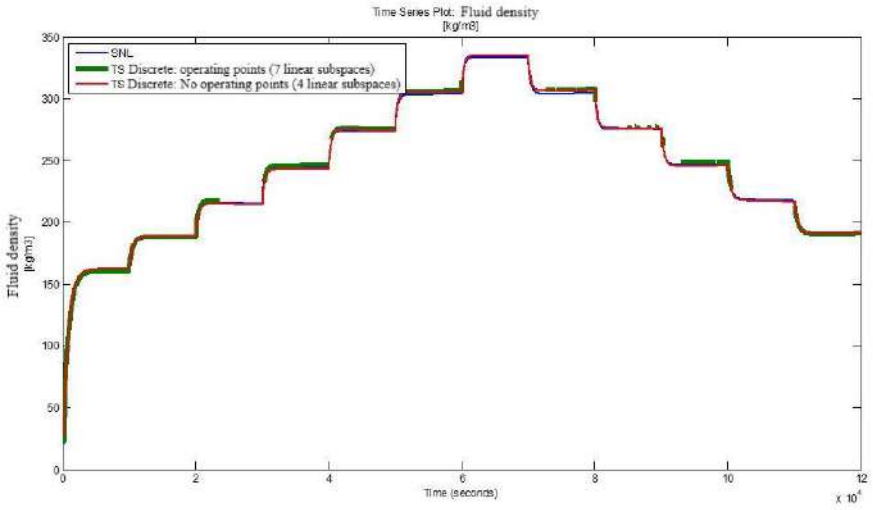

Figure 9. Comparison of the Fluid Density estimation in the Thermoelectric Plant for Case 1.

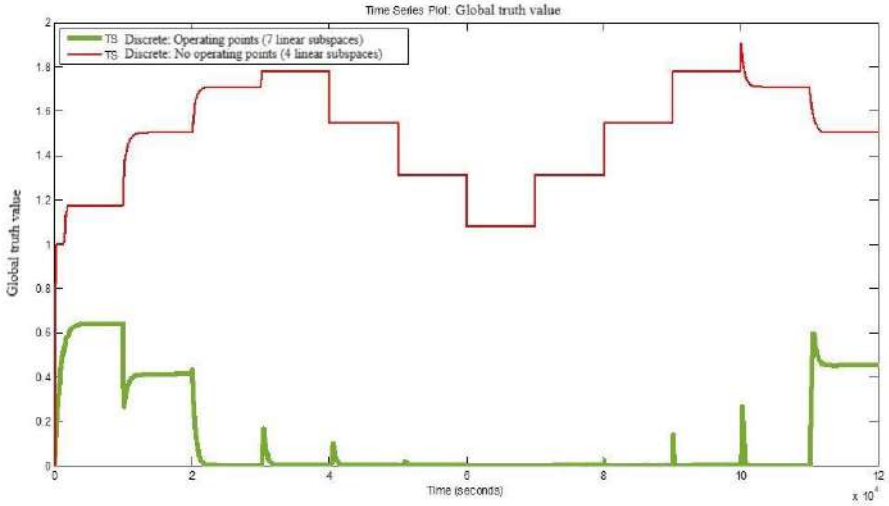

Figure 10. Comparison of the Truth Value of the TSK Models for Case 1.

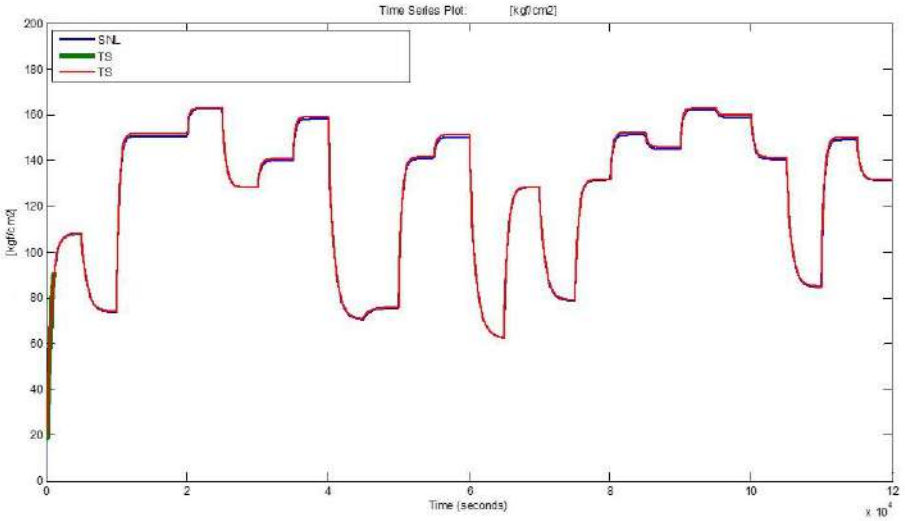

Figure 11. Comparison of the estimation of the Pressure in the Boiler of the Thermoelectric Plant for case 2.

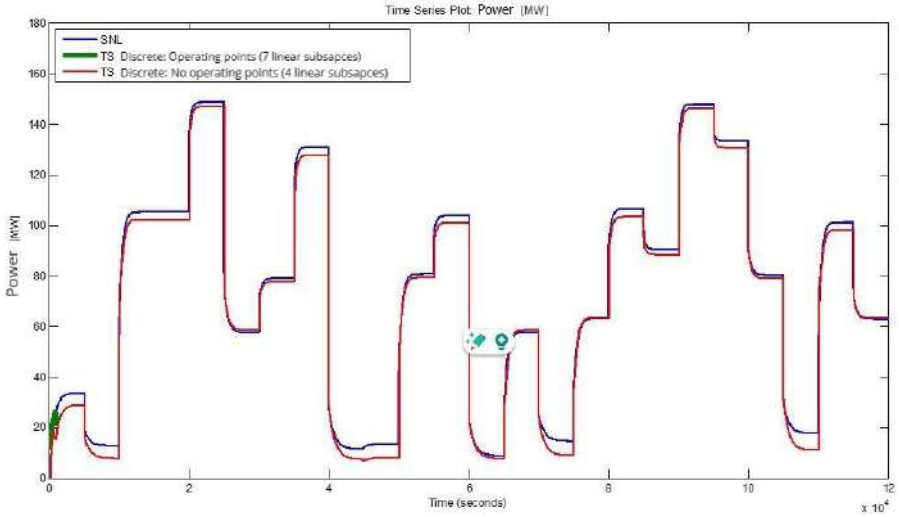

Figure 12. Comparison of the Output Power estimation of the Thermoelectric Plant for case 2.

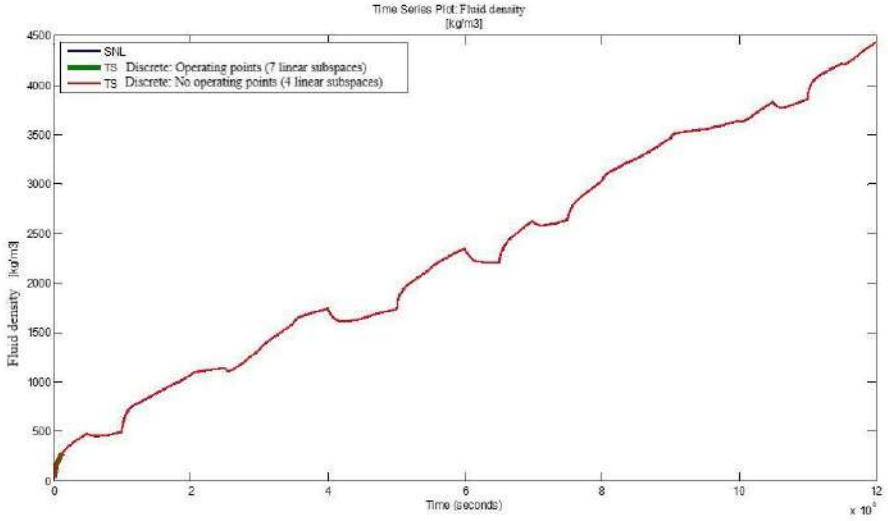

Figure 13. Comparison of the Fluid Density estimation in the Thermoelectric Plant for Case 2.

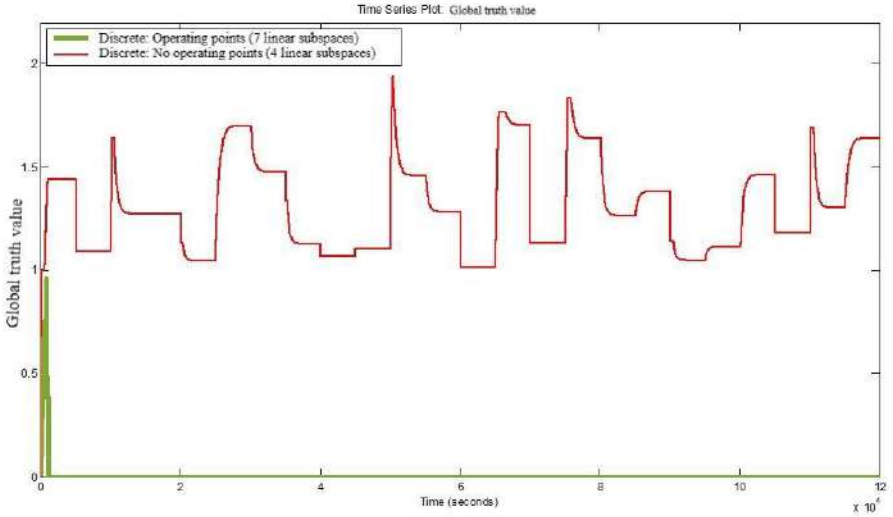

Figure 14. Comparison of the Truth Value of the TSK Models for Case 2.

Table 3 shows the results of the measurement of performance indices for each study.

Table 3. TSK Model Performance Indices.

	TSK Model – 7 Rules				TSK Model – 4 Rules			
	Case 1		Case 2		Case 1		Case 2	
	VAF%	RMSE	VAF	RMSE	VAF%	RMSE	VAF%	RMSE
x_1	Nan	Nan	Nan	Nan	99,96	0,51	99,93	5,08
x_2	Nan	Nan	Nan	Nan	99,05	3,63	97,58	7,19
x_3	Nan	Nan	Nan	Nan	99,94	1,40	100,00	2,80

Table 4 presents the percentage error of the 4-rule TSK model implemented with the proposed algorithm with respect to the nonlinear model, both for case study 1 and case 2.

Table 4. TSK Model Error – 4 Rules Regarding the Non-linear Model.

	TSK Model – 4 Rules	
	Case 1	Case 2
	%Error	%Error
x_1	0.04%	0.07%
x_2	0.95%	2.42%
x_3	0.06%	0.00%

A. Discussion of the Results

For case study 1 (sequence of ascending and descending inputs), in Figures 7, 8, and 9, it is evident that the Discrete TSK model obtained from the points of operation (7 Rules) is not able to follow the sequence of inputs continuously, this is corroborated when analyzing Figure 10, where it is shown that the Global Truth Value of the model becomes zero at multiple points in the trajectory. This cancels the output of the TSK model at those intervals; as a consequence of this discontinuity, it is impossible to calculate the VAF and RMSE performance indices for this TSK Model in case study 1, as shown in Table 3. In contrast, the Discrete TSK Model obtained from the proposed algorithm, if it was able to follow the trajectory imposed by the sequence of inputs, is corroborated in Figures 7, 8, and 9 (red line) and even in Figure 10, in which the Global Truth Value of the model is never canceled. This makes it possible to calculate the VAF and RMSE performance indices, which were above 99.00% and below 3.7 respectively, values that are very close to the ideal case (VAF=100% and RMSE=0).

For case study 2 (sequence of pseudo-random inputs), in Figures 11, 12, and 13, it is again evident that the Discrete TSK model obtained from the points of operation is not able to follow the sequence of inputs, even the performance is still lower than case 1, which is corroborated when analyzing Figure 14 and comparing it with Figure 11; again as a consequence of such discontinuity, it is not possible to calculate the VAF and RMSE performance indices for this TSK Model in case study 2, as shown in Table 3. In contrast, the Discrete TSK Model obtained from the proposed algorithm was once again able to follow the trajectory imposed by the sequence of inputs, which are even more demanding (because they are random), which is corroborated in Figures 11, 12 and 13 (red line), and even in Figure 14, in which the Global Truth Value for this model is clearly never cancelled; As for the VAF and RMSE performance indices, which were above 97.50% and below 7.20 respectively, results that, although they show lower performance than that obtained in case 1, turn out to be extremely interesting given the rigorous sequences of inputs to which the model was subjected.

For both cases, the discrete TSK model obtained from the proposed algorithm was able to follow the SNL satisfactorily.

CONCLUSIONS

In this paper, we have presented an algorithm to synthesize the fuzzy discrete TSK model in linear state subspaces for a MIMO SNL, from the dynamical model in differential equations, without the SNL operating points having been previously defined. The relevance functions in the antecedent are modeled with linear functions. The application of the algorithm to the model of a Thermoelectric Power Plant has been discussed, widely studied in the specialized literature, obtaining satisfactory values in the chosen performance indices (VAF and RMSE). It is expected that this methodology will serve to promote the application of modern trajectory tracking control algorithms based on models in State Space such as: Optimal Control, H∞, Genetic Algorithms, Predictive Control.

REFERENCES

[1] A. Tewari, "Modern Control Design With MATLAB and SIMULINK", Indian Institute of Technology, Kanpur, India, JOHN WILEY & SONS, LTD, ISBN 0 471 496790, pp. 323, 2002.

[2] J. Mendes, R. Araújo, y F. Souza, "Adaptive fuzzy identification and predictive control for industrial processes," Expert Systems with Applications. Institute for Systems and Robotics (ISR-UC), and Department of Electrical and Computer Engineering (DEEC-UC), University of Coimbra, Portugal. pp. 2-15, November 2013.

[3] T. Takagi, y M. Sugeno, "Fuzzy Identification of Systems and Its Applications to Modeling and Control", IEEE TRANSACTIONS ON SYSTEMS, MAN, AND CYBERNETICS, VOL. SMC-15, NO. 1, pp. 116-132, JANUARY/FEBRUARY 1985.

[4] M. Sugeno y G. T. Kang, "STRUCTURE IDENTIFICATION OF FUZZY MODEL", Fuzzy Sets and Systems 28 (1988), pp. 15-33, North-Holland.

[5] K. Mehran, "Takagi-Sugeno Fuzzy Modeling for Process Control", Industrial Automation, Robotics and Arti¯cial Intelligence (EEE8005), Newcastle University, 2008.

[6] S. Kawamoto, K. Tada, A. Ishigame, and T. Taniguchi, "An approach to stability analysis of second order fuzzy systems", in Fuzzy Systems, 1992., IEEE International Conference on, pp. 1427-1434, 1992.

[7] R. Dimeo, K. Y. Lee, "Boiler-Turbine Control System Design Using a Genetic Algorithm", IEEE Transactions on Energy Conversion, Vol. 10, No. 4, pp. 752-759, December 1995.

[8] R. A. Maher, I. A. Mohammed and I.K. Ibraheem, "State-Space Based H∞ Robust Controller Design for Boiler-Turbine System", Arabian Journal for Science and Engineering, ISSN 1319-8025, April 2012.

[9] J. Novak, P. Chalupa, "Predictive Control of a Boiler-turbine System", Recent Researches in Circuits and Systems, ISBN: 978-1-61804-108-1, pp. 383-388. 2012.

[10] J. Wu, J. Shen, M. Krug, S. K. NGUANG and Y. Li, "GA-based nonlinear predictive switching control for a boiler-turbine system", Journal Control Theory Appl, pp. 100-106. 2012.

[11] A. H. Mazinan, "An Intelligent Multivariable Dynamic Matrix Control Scheme for a 160 MW Drum-type Boiler-Turbine System", Journal of Electrical Engineering & Technology Vol. 7, No. 2, pp. 240-245, 2012.

[12] R. D. Bell and K. J. Aström, "Dynamic Models for Boiler-Turbine-Alternator Units: Data Logs and Parameter Estimation for a 160 MW Unit", Deparment of Automatic Control, Lund Institute of Technology. Sweden, December 1987.

[13] J. Castillo, S. Sarmiento, A. Sanz, "ALGORITMO DE IDENTIFICACIÓN DIFUSA PARA EL MODELADO DE UN TANQUE CALENTADO POR SERPENTIN CON AGITACION CONTINUA", Fifth LACCEI International Latin American and Caribbean Conference for Engineering and Technology (LACCEI'2007), 29 May – 1 June 2007, Tampico, México.

ISSN-e: 2737-6419

Athenea Journal
Vol.4, Issue 14, (pp. 22-31)

https://doi.org/10.47460/athenea.v4i14.65

Thermoviscosity mechanism approach in forming fayalite-type ceramic accumulations in particle separators in CFD reactors

Echegaray Alberto
echegaray.alberto@gmail.com
https://orcid.org/0000- 0003-4234-0452
Universidad Nacional Experimental
Politécnica Antonio José de Sucre
Puerto Ordaz- Venezuela

Oscar Dam
oscarcurmetals@gmail.com
https://orcid.org/0002-0594-6757
Universidad Nacional Experimental
Politécnica Antonio José de Sucre
Puerto Ordaz- Venezuela

Received (14/09/2023), Accepted (13/11/2023)

Abstract. - This article presents the fundamental bases to generate knowledge in forming fayalite-type adhesions. Likewise, to determine the conditions that favor the change of viscosity and consequent conditions of the plasticity of the studied system. The analysis focuses on temperatures between 723K and 1023K and pressures above 5 bar. As a result, the formation of adhesions observed in the production process that contain the materials involved and commonly associated with the collision between the particles are estimated, as well as the effect of the different associated energies that arise from this phenomenon. This mechanism may apply to the study of the adhesions of other ceramic materials under thermoplastic conditions with behavior in similar conditions to the studied ceramic system, using the equation modified to that proposed by Mc Lean for thermoelasticity of metals.

Keywords: Thermo-plasticity, relative viscosity, wustite, particle collision, sticking, creep, fayalite.

Enfoque del mecanismo de termoviscosidad en la formación de acumulaciones cerámicas de tipo fayalita en separadores de partículas en reactores CFD

Resumen: Este artículo presenta las bases fundamentales para generar conocimientos en la formación de las adherencias de tipo fayalita. Así mismo, para determinar las condiciones que favorecen el cambio de viscosidad y condiciones consecuentes de la plasticidad del sistema estudiado. El análisis se enfoca en los rangos de temperaturas entre 723K y 1023 K y presiones superiores a 5 bar. Como resultado, se estiman las formaciones de las adherencias observadas en proceso productivos que, contienen los materiales involucrados, y asociadas comúnmente al choque entre las partículas, así como el efecto de las diferentes energías asociadas que se desprenden de este fenómeno. Este mecanismo puede ser aplicable al estudio de las adherencias de otros materiales cerámicos en condiciones termoplásticas con comportamiento similar en condiciones al sistema cerámico estudiado, utilizando la ecuación modificada a la propuesta por Mc Lean para termoelasticidad de metales.

Palabras clave: Termo plasticidad, viscosidad relativa, wustita, choque de partículas, pegado, fluencia, fayalita.

I. INTRODUCTION

These processes tend to operate intermittently during the different iron ore manufacturing processes in which the Prada [1] fluidized bed technology is used for processing. In these processes, de-fluidization is generated, which is caused by the adhesion of partially reduced iron in the fluidized bed D. Fuller [2]. This defluidization is also associated with the formation of accretions on the internal metallic surfaces of cyclones, caused by the collision between the particles at temperatures below the melting point of iron, causing intermittent operation. In this work, the concept of interaction between particles is associated with the apparent viscosity phenomenon. Zhang et al. [3] proposed quantitatively expressing iron-containing particles to resist creep movement in plasticity. It has also been cited that this concept includes the resulting combination of external friction interactions. These cohesive forces include the Van der Waals force, interfacial attraction, and liquid-solid bridges, which are not yet considered to describe particle agglomerations in fluidized bed processes.

That said, the thermo-viscosity approach to the mechanism of formation of adhesions of silicates in a particle separator offers the possibility of explaining the model in terms of the condition that favors a change in viscosity, the consequent condition of plasticity and flow of the resulting materials to form the observed adhesions that contain the involved materials and that are generated. This is based on the release of energy from the particle collision and impact on the interior surface of the particle separator, as well as the resulting temperature that favors the conditions described above. At this point, it is worth an approach to rheology, as the branch of physics deals with the deformation and flow of solid and liquid materials but also applies to complex microstructures, such as silicates.

To study the materials above, those whose viscosity changes with the deformation rate in a specific temperature range are considered and are called non-Newtonian fluids. Therefore, to deal with this apparent discrepancy, it has been accepted that rheology, in general, might be the answer because it accounts for the study of liquids with viscosity dependent on the deformation rate. Its theoretical aspects are the relationship of the flow behavior for the deformation of the material and its internal structure, such as silicates, and the behavior of this type of material that cannot be described by classical fluid mechanics or elasticity.

II. THE PROPOSED MECHANISM

The phenomenon studied is located inside a particle separator inside fluidized bed reactors during the reaction of ferrous oxide to metallic iron, in the range of 500 °C to 800 °C and pressures higher than 5 bar. The adhesions that the reacting materials contain are involved, mainly FeO and SiO2, and are generated as a product of the impact of the particles and the associated energies released at temperatures under the operating conditions described above.

The proposed mechanism aims to consider the condition of the rotating particles within the particle separator. Therefore, the mechanism is based on mathematical formulations to express the phenomena considered in terms of apparent viscosity and consequent plasticity observed in samples of the adhesions of materials with a high presence of ferrous oxide collected from industrial processes. These adhesions were analyzed using Bauman print-type macro etch techniques to observe distribution lines of non-metallic materials and particle flow lines. This provided vital information to understand the proposed mechanism explaining adhesion formation within the particle separator. The formation of adhesions is based on the condition that favors a change in the apparent viscosity and, consequently, the appearance of the condition of plasticity and fluidity of the resulting materials to form the observed samples. The proposed mechanism is schematically described in Fig. 1.

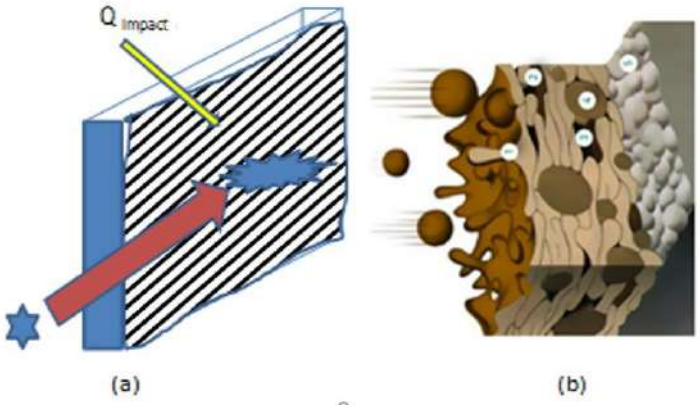

Fig 1. (a) Represents the pattern of impact of a particle against a metal wall (b) Indicates how the layers of the crust are formed by thermo adherence.

In this mechanism, the solid particles heat up during the reaction conversion of ferrous iron to metallic iron. When they impact the surface of the steel and its roughness, they become viscous as a consequence of the impact, it releases enough energy Fig. 1a, and it becomes a material viscous (1), which crawls impelled with the gas flow superimposing the previous imperfections (2) and creating pores (3) and generating the silicates of Fayalite Fig. 1b. Port analogy is a process similar to that of surface thermoactivity.

A. Energy balance

The energy balance was calculated and presented in a previous document by Echegaray [4] and is summarized in Table 1.

Table 1. Energy balance within the particle separator.

Symbol	Energy	(KJ/mol)	(Kcal/mol)
Ec	Impact on cyclone wall	103	30
Ev	FeO vacancies energy	474	113
Ep	Particle's impact	13	3
Ei	Inelastic collision	70	17
Total	Total	660	163

The calculation of the total energy agrees with the reported energies of Gaskell [5] for the Fayalite formation reaction, as well as with the softening point of silica in the range of 2000 ° C of approximately 599 KJ reported by Ringdalen [6] With the total energy calculated of 660 KJ/mol, which exceeds the softening of silica, it is possible to conclude that the formation of Fayalite in the temperature range studied is thermodynamically possible during an intermediate viscous condition.

B. Effect of temperature on apparent viscosity

According to the previous calculations, the total energy balance is 61 KJ/mol over the 599 KJ/mol for the softening of the SiO2 particle formation of the Fayalite silicate, notably coinciding with the range of 61 to 65 KJ/mol considered as compensated activation energy for the deformation-creep of the silicate particles to occur.

To obtain the effect of temperature on apparent viscosity, it is necessary to accept the past energy condition of the solid particles in the gas-solids mixture. These particles that travel in the hot gas stream not only have a suitable thermal condition but, on the one hand, the iron-containing particles are in a transient structure from ferrous oxide (FeO) to iron, which in turn means an additional energy gradient associated with vacancies, which release said energy. On the other hand, among silica particles in a collision path with wustite, these particles are found in conditions of energy levels similar to thermal coating particles projected onto a metal surface at high speeds. With these conditions, the occurrence of the fusion reaction between particles is assured.

C. Adhesions of silicate by action of fluence

Having assumed the formation of a viscous phase formed by FeO-SiO2 as essential components for the formation of silicates, together with the additional presence of MgO and metallic iron, it is possible to assume that the viscous phase was formed under a gas velocity of 75m/s entering each cyclone at that time, the appearance of a deformation force will create a thermo-viscosity situation. The presence of the deformation force on the viscous silicate led to the consideration of a combination with a creep regime.

Considering the creep regime, a dependent temperature effect, it is necessary to consider the melting temperature (Tm) of the species involved. In this case, the species in question is metallic iron. This relationship was driven by the different flow rates for metal powders, covering roughly the metal temperature ranges from 0 to 1 times Tm. This range has a lower range of 0.3-0.5 of the melting temperatures of the metal considered, for which it was defined as a creep dependent on the logarithmically of the temperature, which is governed by an Arrhenius factor, similar to liquid metal streams. The temperature and tensile creep stress dependence have been studied in α-ferromagnetic iron in the temperature range 620 °C -700 °C.

The activation energies for creep can be made using the slope change method. In this way, it is shown that the activation energy compensated by the mathematical simulation model is essentially independent of the initial stress and of the deformation up to the solidification point. With this method of slope change, an activation energy compensated by the model of 65 kcal/mol is obtained. On the other hand, when graphing the logarithm of the variation of the deformation paid by the model versus the inverse of the absolute temperature, it allows to obtain a straight line that represents an activation energy compensated by the model of 62 kcal/mol, K Murty et al. [7]. These values are essentially by the self-diffusion value in this temperature range.

D. Thermoplasticity and fluence relationship

The activation energies, both the creep and the self-diffusion, indicate that the creep process mechanism is controlled by diffusion and, therefore, by a non-conservative dislocation movement. This means that at the speeds of deformation and temperatures used, the average vacancy concentration is only a slight disturbance of the equilibrium vacancy concentration in the tested undeformed samples. The creep data available on some FCC metals shows that obtaining a reasonable energy estimate for the movement of vacancies is possible. From a thermo-mechanical approach, in this work, it was possible to establish the physical meaning of the energy released by a defined particle size within the separated particle. Chica et al. [8] explain that it starts from Cauchy's first law and multiplies both sides by the viscosity (v). Rearranging the terms, we finally get that:

$$\frac{D}{D_t}\left(\frac{v^2}{2}+\varphi\right)=(\nabla.T).v+T:\nabla v \quad (1)$$

The product $\nabla \boldsymbol{v}$ represents viscous dissipation Ev. The formation of accretions in the form of shells in the cylindrical zone in the temperature range above 600 °C and pressures above 10 bar is possible in fluidized bed processes when working with molecular weights in the gas of 10 gr/mol. Therefore, the appearance of thermoplasticity in the studied temperature range 600 °C (873K) to reach the melting point of iron requires validation since, from the point of view of the collision between particles, enough energy may be released to go to the point of thermoplasticity, that is, it starts the process of softening the particles.

E. Effect of temperature on apparent viscosity

Once the apparent viscosity of the studied components has been identified and quantified, as well as the participation of creep in the proposed mechanism, the next step is to determine the effect of the critical temperature on the occurrence of thermoplasticity. As mentioned above, in the mechanism studied, there is an initial conditioning of the partially reduced iron oxide due to its heating by the gas flow. This precondition has been related to the adherence tendency of the minerals used in fluidized bed reduction processes. This is a particular tendency of the different minerals and their mixtures used in the process. In Fig. 2, the transition of the formation of the metallic iron step is shown. This figure shows the effect of the formation rate of metallic iron, opposite to the reduction of ferrous iron, on the critical adhesion temperature during the passage from wustite to iron. Depending on the reduction stage, hot particles naturally develop an active sticking tendency or sticking potential.

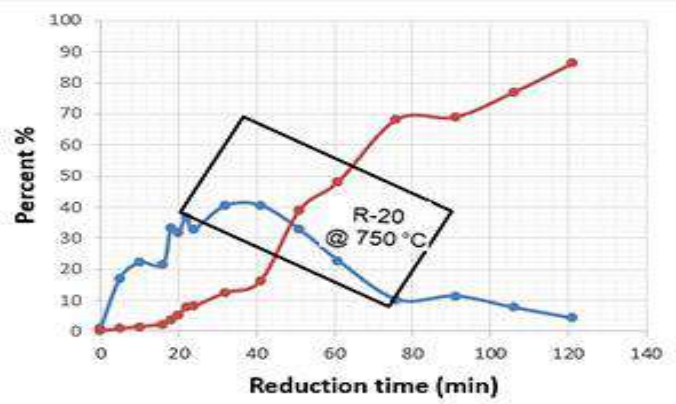

Fig 2. Transformation of ferrous iron into metallic iron in the studied area.

The data for the elaboration of Fig. Three were obtained from industrial tests used in a C F. D plant using mixed Venezuelan and Australian mineral mixtures that are 100 percent Australian. From this figure, it is possible to estimate the ranges of the temperature values for the occurrence of sticking of iron particles, partially metalized as a function of the formation of metallic iron of the particles during their transfer into the particle separators. The temperatures obtained can be assumed as actual, working, or operating temperatures. This temperature creates an activated state of the particles, prone them to the appearance of different stages of the sticking phenomena, such as bogging or particle agglomerations in the fluidized bed, crustal adherences in the upper cylindrical section of the particle separator sand sintering in the returning particles in the separator leg in the lower portion.

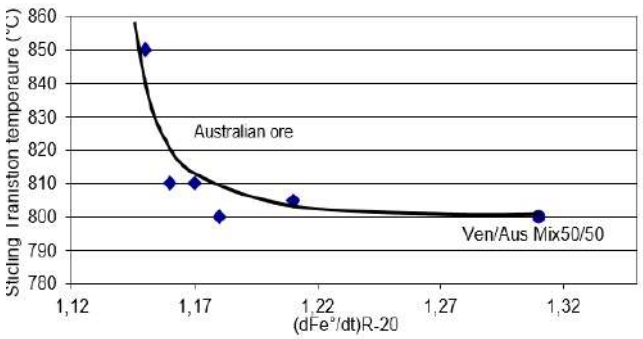

Fig 3. Effect of the metallization rate on the critical adhesion temperature.

This activated adhesion potential, thus developed by the partially reduced iron oxide particle, enters the particle separator on the path of eventual collision with the clean steel surface during initial accretion formation or further accretion development. This kinetic behavior can be expressed mathematically according to the following equation,

(T) real operation = 3.987, (dFe°/dt)2 -9.974,9 (dFe°/dt) + 7027,8 (2)

With a correlation R^2 of 0,7684, representing the reliability of industrial data more significant than 85%, it is considered very acceptable because it is industrial data.

III. METHODOLOGY

At this point, the appropriate theoretical and thermodynamic basis for the proposed mechanism has been established, and the empirical relationships between the critical temperature variables of adherence, viscosity, and creep of the silicates formed during the collision of solid particles as well as with the impact that exists between the particles and the surfaces of the particle separator two. The following sections describe the steps to obtain the presented results.

IV. RESULTS

A. Sample preparation

To corroborate the observed system, solid industrial samples were taken from the accretions formed inside the particle separators, as shown in Fig. 4. These samples were cut, roughened, and etched with a 12% sulfuric acid solution to reveal the flow lines of the formations of the different layers in the opposite direction of the gas flow entering the mouth of the cyclone separator.

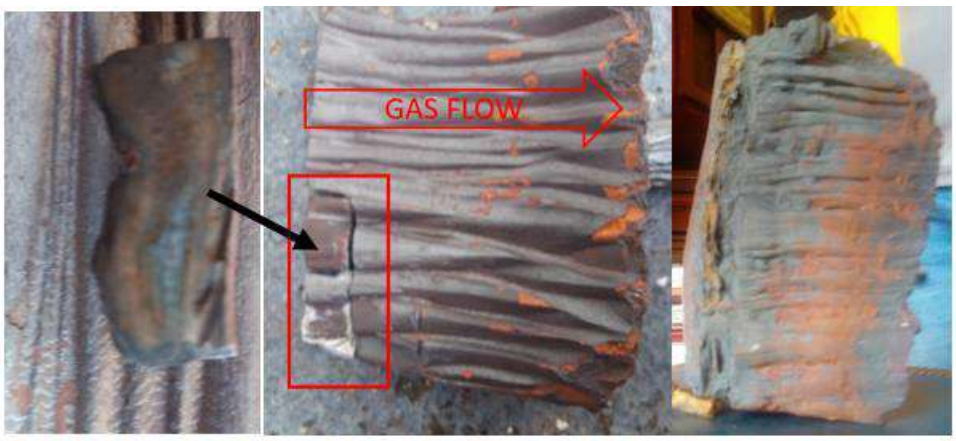

(a) (b) (c)

Fig 4. Sample of gas flow accretion and creep lines (center), samples taken from the thinner incoming tail, Image (a) shows flow line and layers of deposited material when attacked with 12% sulfuric acid (side of the separator on the right edge) and the side of the gas to the left of the image (b), which shows the accelerations formed by the collision between particles, the image (c) shows the shape of the flow lines of the adhesions in the metallic crusts, at the point where the impact speed decreases. This proposed mechanism complies with thermodynamics and the process conditions for accumulations.

B. Proposed coefficient for iron oxide dust

Depending on the temperature range, the materials have a thermo creep constant McLean [9] 0-0.3 TM, 0.3-0.5 TM, 0.5-0.9 TM, and 0.9-1.0 TM. Where TM is the melting temperature of the pure element, in this case, iron; based on this information, the following graph was obtained.

Table 2. Comparison of obtained calculation results.

Temperature (°C)	K Termo Creep	Temp. Creep
461	0,3	460
700	0,5	767
1400	0,9	1381

C. Influence of temperature on the thermal adherence constant

The value of the adhesion coefficient in the temperature range between 600°C and 700°C oscillates between 0.478 and 0.514 with a correlation of 0.977 for ceramic materials. These values are based on the range of coefficients proposed by McLean for metals in a diffusion-controlled creep process to consider a similar flow in liquid metals. These values are assumed to be related to a combined effect of the working pressure on the temperatures, which also affects the particle velocity, gas molecular weight, and oxide properties, such as a plastic-activated stage for any sticking tendency.

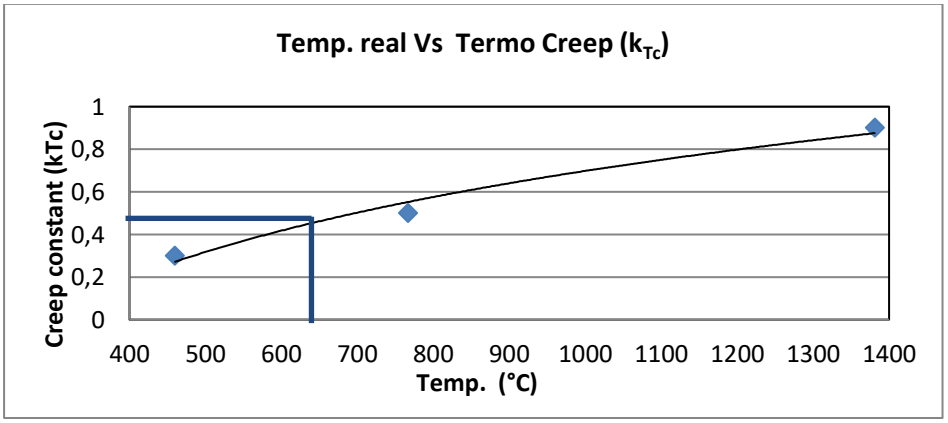

Fig. 5. Result of the thermo creep constant when working in a temperature range from 600°C to 700 ° C of 0.4784.

Once the operating temperature is obtained, the thermal creep constant is estimated. This value will be crucial to know the temperature for the mathematical simulator, as shown in equation 3. In this equation, KTc is represented as the constant of thermo creep, and Tr is the actual operating temperature in degrees centigrade. This gives a dimensionless value.

$$K_{Tc} = 0.5491 * \ln(Tr) - 3.095 \quad (3)$$

Using the temperature difference mentioned above, for the occurrence of thermoplasticity in the considered system, in the temperature range 600 ° C (873K), to reach the melting point of the newly formed iron required, the value of the system's thermo-creep constant with a value of 0.478. This value represents a modification of the equation described by McLean applied to ceramic systems. Then, the modified equation to define the appearance of yield stress in the study system can be represented by Equation 4 and Figure 6.

$$Tc = 2.0921*Tr - 1E\text{-}12 \quad (4)$$

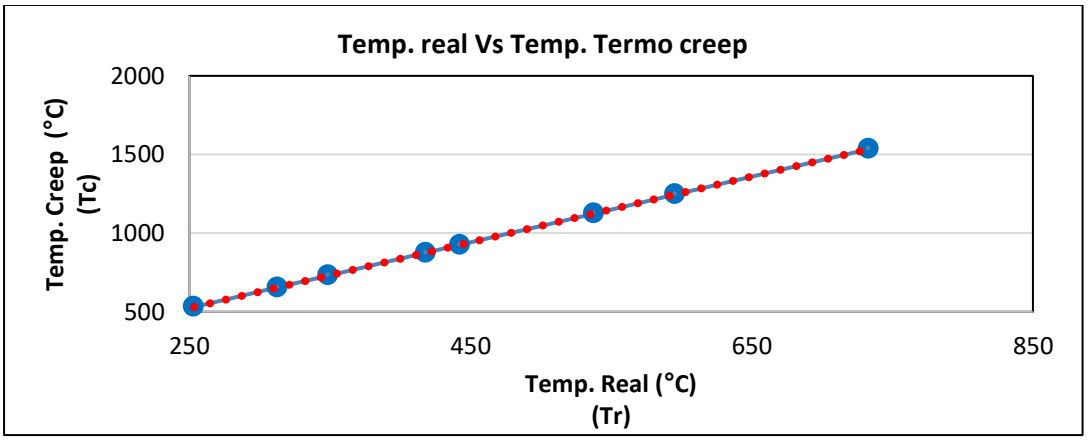

Fig 6. Formation of thermal adhesion as a function of accurate operating temperatures.

D. Activation energy in the study system

The formation of adhesions in the form of shells in the cylindrical zone in the range of temperature and pressure studied is possible in fluidized bed processes when working with molecular weights in the gas of 10 gr/mol. To develop the critical temperature for the thermoplasticity of the partially reduced particle, it is necessary to assume a specific temperature gradient between the hot gases and the solid particle. Therefore, this investigation took a difference of 30 degrees Celsius for heat transfer.

$$logK = \log A - \frac{E_A}{R} * \frac{1}{T} \quad (5)$$

Figure 7 shows the thermal creep temperature on the vertical axis as a function of the thermal creep constant used to visualize the change in temperature as a function of the Arrhenius activation energy.

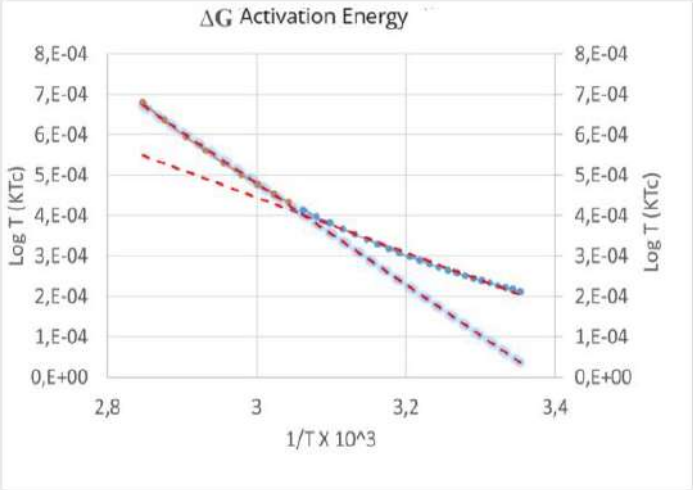

Fig 7. Activation energy through the Arrhenius relation
Diffusional Control CD; CQ Chemical control; CM Mixed Control

In the case of collided particles, the activation energy values for the temperature range studied help identify the predominant mechanism: dysfunctional control, mixed control, and chemical control.

The values obtained for the different mechanisms are as follows:

1.-Diffusinal Control
Log K = -0.013 * 1 / T + 0.0045 (6)
3.- Mixed Control
Log K = 0.052 * 1 / T + 0.0038. (7)
2. Chemical Control
Log K = -0.0008 * 1 / T + 0.0028

The influence of temperature can be worked by following the particle collision theory described by Arrhenius. In these graphs, chemical control is generated where the Bogging formation of accumulations in the bed can occur. The first hypothesis is rectified: a diffusion control where occurs sintering and finally, a mixed control is affected by the change in temperature and the constant of the thermal creep, the activation energy is of the dysfunctional control 5.949 Kcal/mol pending 1.3 $X10^3$; Chemical control 3,661Kcal / mol pending 0.8X 10^3 and mixed control 4.805 kcal/mol pending 1.05$X10^3$.

.

CONCLUSIONS

1. The application of particle collision theory has helped determine the energies generated for the formation of adhesions in the particle separators in the range of 600 °C to 700 °C to determine the formation of fayalite in systems that combine the presence of ferrous oxide, silica and the presence of magnesium oxide.
2. The values of the adhesion coefficient for ceramic systems, such as the one studied. Within the temperature range between 600 °C and 700 °C, it oscillates between 0.478 and 0.514 with a correlation of 0.977. These values modify what Mc Clean proposes for metals by the range of coefficients presented and already indicated and are applied in a diffusion-controlled creep process to consider a similar flow in liquid metals for the case of thermospray.
3. This theoretical principle has made it possible to determine a creep temperature constant that modifies McLean theory for ceramic types of metals when the energy released inside the particle separator exceeds the transformation value of solid oxides to liquid and is sufficient so that the oxides studied are susceptible to thermo-viscosity and consequent plasticity.
4. The results summarize the summation of the energies released inside the cyclone separator, which is 660 KJ/mol higher than the 599 KJ/mol required to melt silicon oxide at 2000 ° C.
5. Applying the Arrhenius equation, it is possible to determine the activation energy for chemical (CQ), dysfunctional (CD), and mixed (CM) control. As a result, an activation energy of 5.94 kcal/mol CD, 4.81 kcal/mol CM, and 3.66 kcal/mol CQ with a total activation energy of 14.41 kcal/mol for the formation of fayalite, a value very close to the theoretical value.

RECOGNITION

The authors are incredibly grateful to the Graduate Research Directorate at UNEXPO Puerto Ordaz for the opportunity to carry out this research related to a focus on the thermoviscosity mechanism in the formation of fayalite-type ceramic accumulations in particle separators in CFD reactors that occur at temperatures below the eutectic point.

REFERENCES

[1] Á. Prada, (2014). Estudio aglomeración lecho fluidizado. 3-52.
[2] D. Fuller (1965). Fenómenos de Sinterización de finos en proceso de reducción directa. Puerto Ordaz
[3] Y. Zhang., Z. And, Ed Z. Guo., (2015). Apparent viscosity measurement of iron particles. 6th International Symposium on High-Temperature Metallurgical Processing, 559-564.
[4] A. Echegaray (2021). Balance de energía en la formación de fayalita sub-eutéctica a altas presiones en separadores de partículas. ORCID 0003-4234-0452.
[5] D. Gaskell (2003). Introduction to the Thermodynamics of Materials. New York: Taylor & Francis 695-696
[6] E. Ringdalen (2016). Softening and melting of SiO2 are essential parameters for reactions with quartz in Si production 43-44.
[7] L. Murty, M, Gold, & A. Ruoff. (1970). High-Temperature Creep Mechanisms in an Iron Alfa and Other Metals. 41(12), 4917-4937.
[8] L. Chica, O. Bustamante and A. Barrientos (2013) "Disipación de energía mecánica en la descarga de un hidrociclón: Nueva estrategia de modelo" revista Dyna año 80 Nro. 181 p.p 136-145 Medellín.
[9] D. McLean. (1966). The Physics of high-temperature creep in metals. Science, 1-33.

The Authors

Alberto R Echegaray R, Metallurgical Engineer, Graduated from Unexpo Puerto Ordaz of Venezuela in 2002. Master Science in Metallurgy and Postgraduate in Simulation, Energy Efficiency, Specialist in Maintenance Management. Studying a PhD in Engineering Science at Unexpo. Member of the engineering college. I have worked since (1998) in Fior de Venezuela. In (2000) I moved to the start-up group of Finmet Technology in Orinoco Iron (Orinoco Briquetera) with the position of operation technician, technical assistant, and later a Specialist in level IV process. I am currently working in the Energy Management department attached to the Presidency.

Oscar G Dam G, Metallurgical Engineer graduated from Universidad Central de Venezuela 1972 Master Science in Metallurgy and Diploma (DIC) Graduated from the Imperial College of Science and Technology 1977, England Doctor in Metallurgy graduated from the University of London in 1983. Department of metallurgy at the Instituto Experimental de Guayana since 1978. Postgraduate professor in materials science at Universidad Central de Venezuela and at the Universidad Experimental de Guayana since 1984, external tutor for postgraduate studies at the Instituto Venezolano de Investigación Científica.

ISSN-e: 2737-6419

Athenea Journal
Vol.4, Issue 14, (pp. 32-44)

https://doi.org/10.47460/athenea.v4i14.66

Mathematical model of the convective behavior of climate variability applied to a cubic Hadley cell

Girón Mara
https://orcid.org/ 0000-0001-9215-1807
maragiron.777@gmail.com
Universidad Politécnica Antonio José de Sucre,
UNEXPO
Puerto Ordaz-Venezuela

Received (12/10/2023), Accepted (29/11/2023)

Abstract. - A mathematical model is presented to assess the impact of climatic anomalies and convective behavior on climatic variability at the Earth's surface, focusing on soil-atmosphere interaction. This model is applied within a control volume covering the Hadley cell, allowing for the verification of convective coupling and prediction of the effects of the studied climatic variation. The mathematical analysis delves into the soil-atmosphere interaction within the control volume, quantifying variations in water evaporation levels in bodies of water and soil, water vapor content in clouds, adiabatic gradient in the atmosphere, relative humidity, and condensation, taking into account average solar radiation. This developed model is a robust foundation for reproducing convective climate effects, pinpointing coupling forces, and validating models in local climate studies.

Keywords: Soil-atmosphere Interaction, Hadley cell, Climate variability, DECASAI.

Modelo matemático del comportamiento convectivo de la variabilidad climática aplicado a una celda cúbica de Hadley

Resumen: Se presenta un modelo matemático que aborda la influencia de anomalías climáticas y el comportamiento convectivo en la variabilidad climática en la superficie terrestre, con especial énfasis en la interacción suelo-atmósfera. Este modelo se aplica en un volumen de control que abarca la celda de Hadley, permitiendo la verificación del acoplamiento convectivo y la predicción del impacto de la variación climática estudiada. El análisis matemático se centra en la interacción suelo-atmósfera dentro del volumen de control, cuantificando la variación en los niveles de evaporación del agua en cuerpos de agua y suelo, la cantidad de vapor de agua en las nubes, el gradiente adiabático en la atmósfera, la humedad relativa y la condensación, considerando la radiación solar promedio. Este modelo proporciona una base sólida para la reproducción de efectos convectivos del clima, localizando la fuerza de acoplamiento y validando modelos en estudios climáticos locales.

Palabras clave: interacción suelo-atmósfera, celda de Hadley, variabilidad climática, DEACISA.

I. INTRODUCTION

Since MTC UNAM has recognized it as GLACE, the atmosphere, soil, and vegetation systems are dynamically related to the physical processes that generate the transfer of heat energy and water mass across the Earth's surface [1], as well as all processes and mechanisms of convection of atmospheric heat obey the physical laws of thermodynamics, this work is framed within the same principles and concepts.

This paper presents the mathematical model as a general development for comparing the consulted models' approaches to the atmosphere-soil-ocean interaction models and the one proposed. It shows the general methodology of the mathematical model named DECASAI in the control volume and its boundary conditions with the proposed equations. Finally, the results are presented with a case study to demonstrate the application of the relationship of the equations and quantification of the variation of the evaporation rate in a prolonged time of a climatic anomaly and Conclusions on which possibilities of lines of research of the climate change.

II. DEVELOPMENT

All processes and mechanisms of convection of atmospheric heat obey the physical laws of thermodynamics, and the interaction of these allows related mathematical equations to be formulated to study the soil-atmosphere interaction, focusing on the atmosphere as a heat engine. With this concept, it is possible to find a scientific explanation for the behavior of these effects and their relationship with climate variability. However, to date, the documentation consulted on the subject [2], [3], [4], [5], [6], [7], [8], [9], of the behavior applied so far, in the atmosphere-earth system focused on predictions and the history of the occurrence of climate variability as is the case of the models.

Atmospheric phenomena are strongly influenced by the distribution of topography and vegetation on the continent's surface. For this (climatic) model, the spatial configuration (domain: Continental and Regional) and the physics of the model and establishment of the boundary conditions and model equations, the latter being one of the objectives of this study. The physical processes considered were the surface flows between atmosphere-soil, soil hydrology, courses within the border layer, radiation, the physics of explicit humidity, deep convection, and clouds of little vertical development established within the troposphere.

A. Model definition

For the development and application of the model, the Hadley Cell [10], is taken as a control volume located within the tropics around the Equatorial zone. The climatic characteristics of the convergence zone intertropical (ITCZ) for the areas of the American continent and Monsoon for the African and Asian Continent. The representative developed model for this study is convective cells of air masses [11], and the influence of the hydrological cycle in a given region. Because atmospheric convection is often caused by variations in the temperature and humidity of the air near the surface, it is expected that convection is a phenomenon in the behavior between soil moisture and clouds.

For the boundary conditions of the control cube, the convergence of the trade winds is considered, considering the climatic anomalies as a case study of the ENSO (El Niño Southern Oscillation) phenomenon [12], [13]. Physical parameterizations, including temperature, wind speed, and variables, to study the relative influence of convection and soil hydrology aim to improve vulnerability studies of a particular region. The following considerations inside the Hadley cell are visualized for model definition purposes, as shown in Figure 1, including air flows over a water body air profile. In open spaces such as seas, rivers, and lakes, natural or artificial, such as dams, although generally accepted to be turbulent flows above surface waves, are not well known yet.

As infinitesimal waves are studied, it is an excellent approximation to consider mean flow profiles above flat plates [14]. The wind blows over the water's surface. The air viscous effects induce a shear velocity profile in the water. This effect is considered to generate boundary layers with high shear to develop immediately the air-water interacting zone. Consequently, this air-water interacting zone, not quantified in this work, is unstable, leading to small waves on the water surface. Friction stresses are not considered; neither is the Coriolis Effect nor air velocity.

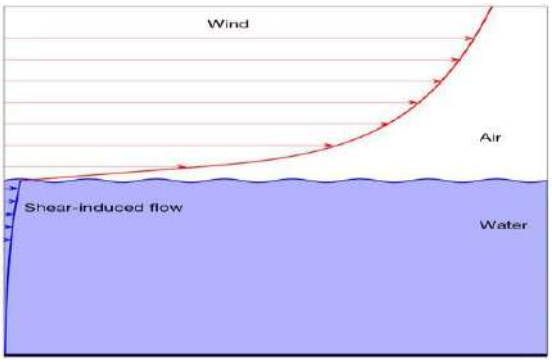

Fig. 1. Coupled shear flows. The air-water interface is unstable with the wind-blowing effect, and small water waves are grown in the wind-blowing direction [15], [16].

The theoretical study of the generation of water waves by wind relies on the hypothesis that the mean velocities and profile shape are in the turbulent air and the water interactive zone. Thus, it is regarded as a parallel shear flow, as shown in Figure 2.

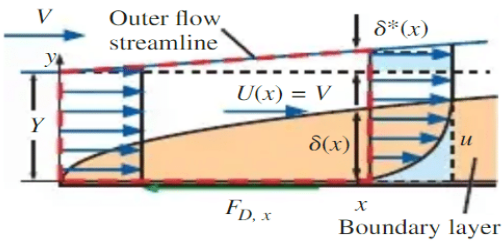

Fig. 2. Wind blow stream effect on a flat plate surface acting in the boundary layer [17].

Therefore, the velocity profile shape is considered as an independent variable. In the model application section, values concerning the mean flows used for air and water are given and used. These depend on the local environmental characteristics. In the present work, the model developed by van Driest is considered suitable for the case study analysis below. The analogy is made assuming the following aspects, as shown in Figure 3:

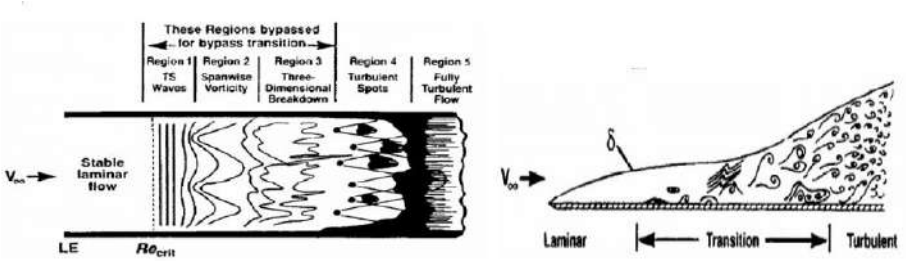

Fig. 3. Schematic of boundary layer transition with the different phases indicated. Copied from [18], [19].

The boundary layer displacement thickness $\delta *$, which quantification is not considered in this work, is given by:

$$\delta * (x) = 1.72x\sqrt{Rex} \quad (1)$$

The boundary conditions can be applied for flow over a flat plate, considering the soil surface layer of -5cm to 10cm above and establishing standardized soil porosity values.

III. METHODOLOGY

Considering thermodynamics, for the developed model, the thermodynamic and kinetic relationships of thermal imbalances in the atmosphere, as well as semi-empirical parameterizations. Viewing the data of the averaged climatic variables, the laws of hydrostatic balance and continuity equation, and the energy balance model.

A. Experimental methodology of the DECASAI model development

The methodology consists of establishing the control volume within the Hadley Cells as a reference base configuration and the boundary conditions or changes in the parameterizations used to evaluate the effects of said changes on the regional climatology. The first step is establishing the configuration of the domains, continental and topography, and the conditions inherent to the study area, its geographical and spatial location. The second concerns boundary conditions and the climatic data involved in each face of the assumed control volume. The third is the base configuration for the representation of the climatology of the area. The fourth is establishing the related equations following the thermodynamic and kinetic parameters.

The methodology is based on the logic to Determine Analysis and Method) the (DAM Pyramid) [20], starting with variables and assumed parameters, followed by the thermodynamic and kinetic laws and principles, the formulation of equations, the incremental relationship of the calculated effects, the validation of the results and their application to the real world with regards to ecosystems vulnerability.

B. Model description

The DECASAI model considers vertical winds, and the following variables are shown in Table 1.

Table 1. Meteorological variables considered in DECASAI.

Symbol	***Description***	***Unit***	***Symbol***	***Description***	***Unit***
Tg	Air Temperature	*℃, °F, °K*	r	Local Radiation	W/m^2
Ta	Water Temperature	*℃, °F, °K*	H	Local Soil Moisture	*%*
Te	Temperature Anomaly (Enso)	*℃*	Vv	Wind speed	*Km/h*
Tm	Medium temperature	*℃*	h	Reference Atmospheric Height	*mm Hg*
pa	Atmospheric pressure	*Kpa, Atm, mm Hg*	L	Length Traveled For Wind	*cm*
Pvs	Water/Soil Vapor Pressure	*mm Hg*	A ca	Body of Water Area Volume of water	km^2
Pva	Water/Water Vapor Pressure	*mm Hg*	Va	Volume of water	m^3
Vl	Specific Volume of Liquid	*cc/g, cc/mol*	Ab	Bio diverse Area	km^2
Q	Water Flow Bio diverse Area (biomass)	m^3/s	t	Anomaly Duration (Enso)	*months*

Source: Author

The characterization of the system includes part of the parameters used in the predictive models, such as the value of the thermal anomaly detected in °C, wind speed of climatic anomalies (ENSO), the value of water vapor towards the clouds, relative humidity of the selected regions (vulnerable to its impact). The thermodynamic and kinetic characterization include the corresponding parameters, such as physical characteristics of the fluids involved (air, water, water vapor), characteristics and variations of temperature conditions with height and pressure of the atmosphere, characteristics of vulnerable affected soils and their relationship with the humidity necessary to maintain biodiversity, Affected areas that host water bodies of reservoirs and water basins, biodiverse areas considered as microclimates. Formation of water droplets, the behavior of relative humidity for precipitation, and the calculation of the amount of entropy exchanged between the air masses involved. Thermodynamics of Soils for the effect of water evaporation from the bodies of water considered and the impact of moisture evaporation from the associated soils.

To define the base configuration, it was necessary to analyze the patterns of meteorological variables, such as relative humidity, air temperature, atmospheric pressure at sea level, solar radiation, and wind speed. Commonly, these variables have a daily cycle associated with changes in the winds of the intertropical ZIT zone due to their location near the equator. The intensified trade winds of the studied control volume are also induced.

C. Initial and boundary conditions

The development of the model focused on the understanding of the Hadley cells, analyzed as a convective behavior at a height of 10km-20km (at the troposphere level). Studying this effect in more detail in the Equatorial zone, presenting the domains in dry and humid regions on spatial scales of 12km x 12km x 12km (see fig. 4a and 4b).

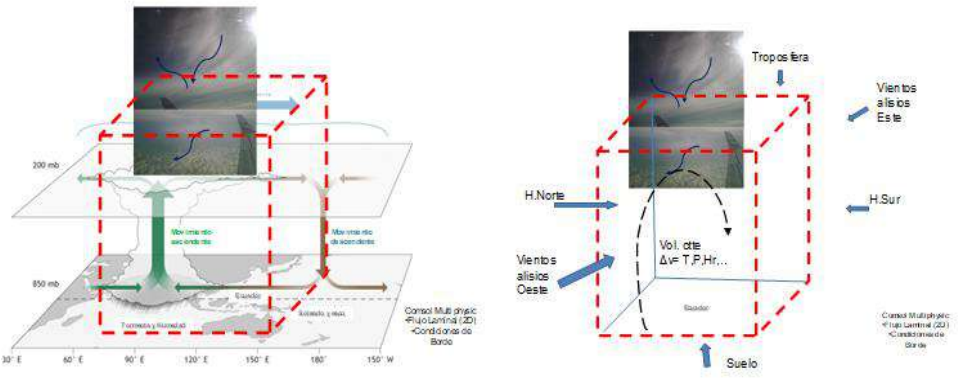

Fig. 4. Control volume (a) convection inside the Hadley cell; (b) Control Volume on the Hadley Cell. Source: Author.

From this control volume, the analysis was carried out during climatic anomalies such as drought or rain. Based on the Onsager model and theory, the convective aspect is incorporated into the control volume for simulation in three axes but oriented and limited to the interrelationships of the same variables within the control volume. The boundary conditions are analyzed from this control volume (Fig. 5a, 5b). Based on the model, the presence, effect, and direction of the characteristics of the six faces of the presented cube are shown.

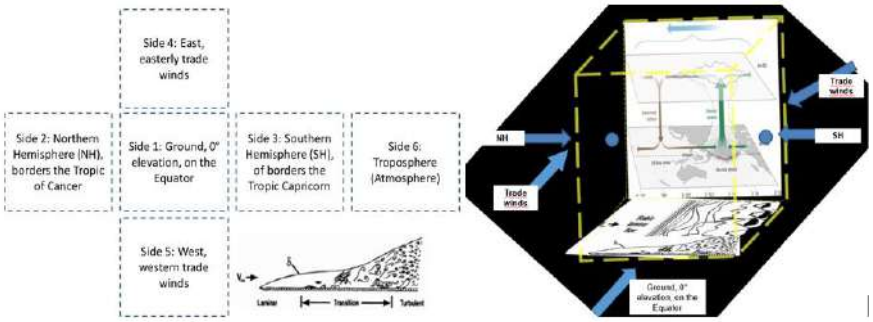

(a) (b)

Fig. 5. Control volume (a) Control volume sides (b) Control volume established over the Hadley cell.
Source: Author

D. DECASAI geographic characteristics

The geographic information in the model and relevant meteorological meshes. These parameters are the size of the body of water (reservoirs, lagoons, dams); Biomass size (surrounding area where that body of water is located); Height above sea level (msnm); Annual average of soil temperature (it is considered that the diurnal cycle does not affect variations in soil temperature, it is assumed constant); Solar radiation (Albedo is not viewed as it is a secondary parameter that depends on land use); Wind speed (average speed under normal conditions and with anomalies-ENSO, Monsoon, among others).

E. Technical characteristics

Surface temperature; speed and direction of zonal and southern winds; Vertical wind speed and direction (m/s); Configuration of 2 domains (Continental, Regional); Surface temperature (°C, °K, °F), airflow speed, assumed about 20km/hr-22km/hr, to Northern Trades, >117km/hr as a Tropical storm.

The equations involved in the DECASAI model are the following:

F. Water bodies evaporation

Water evaporation is calculated in water bodies with increasing entropy as uncompensated energy. For this purpose, the Nusselt number (Nu) was used to measure the increase in conductive heat transmission with Nu = Nusselt number (dimensionless number); h= convection heat transfer coefficient (W/m^2K); L = characteristic length with the default value L= 1; k= thermal conductivity coefficient of the fluid (W/m.K). In the case of flat plate forced convection in laminar flow, at a distance x downstream of the plate edge, it is given by the Nusselt number represented as the function of the Reynold number (Re) and the Prandtl number (Pr), Ʊ= viscosity of air (cc/sec), in a simple way, $Re < 5 \times 10^5$, $Pr > 0.6$.

$$Nu = \frac{\mathrm{hL}}{\mathrm{k}} = \mathrm{f}(\mathrm{Pr}, \mathrm{Re}) = 0.332 * Re^{1/2} * Pr^{1/3} * Ʊ \quad (2)$$

The obtained Reynolds number is for turbulent flows, ρ= fluid density, L= length (cm), Sa= air volume (m/sec), v= air speed (m/sec), being: ρ= density of atmospheric air at water level 15°C=1225 kg/ m 3; Prandtl number "Pr" (dimensionless number) is taken Pr air = 0.71; α = thermal diffusivity heat transfer coefficient, Ʊ= moment of diffusivity, Ʊ= viscosity of air (cc/sec), The water vapor pressure above the ground (Pvs) reaches the atmospheric pressure at sea level at 760 mmHg.

$$\frac{\mathrm{Pvap}}{\mathrm{water}} = \mathrm{Pvv} = 0.2473 * \frac{\mathrm{Pv}}{0.113} \quad (3)$$

The volume occupied by air at the temperature of T_o=273.15°K is V_o=3.95.At, at this temperature, it is assumed that the amount of water vapor is minimal. We have P_v= water vapor pressure= 4.44 (gr/cc) and T in [K]. The viscosity ratio (Ʊ)/Diff) is deduced from,

$$\frac{\text{Ʊ}}{Diff}\left(\frac{cc}{s}\right) = Hr(\%)/Tair(°C) \qquad (4)$$

The mass transfer coefficient (hp) relates the rate of mass transfer, the mass transfer area, and the change in concentration,

$$\text{hp} = \left(0.664 * (\text{Ʊ})/\text{Diff})^{1/3} * Re^{1/2}\right) \qquad (5)$$

Where (Ʊ)/Diff= air viscosity ratio (cc/sec), Re= Reynolds number. Constitutive laws of matter in equilibrium, the law of Ideal Gases. They relate the dependent variables to the independent ones. Where: P= absolute pressure (measured in atmospheres), V= volume (expressed in liters), n= moles of gas, T= absolute temperature, with a molar mass for air M= 0.029 kg/mol, R= constant universal of ideal gases (0.082 atm.L/mol.K), R = Ru, M = 287 (J/kg.K), with the universal gas constant Ru = 8.314 (J/mol.K). Convection arises naturally in the atmosphere. This process is governed by the Ideal Gas Law, which describes the relationship between the pressure, volume, temperature, and quantity (in moles) of an ideal gas such that the amount of evaporated water (ECwater) given in gr/h.\ m^2, would be:

$$\text{EC}_{\text{water}}\left(\frac{\text{gr}}{\text{h } m^2}\right) = \text{hp} * \frac{\text{Pvv}-\text{Pv}}{0.082*(\text{Tm}+273)} \qquad (6)$$

E(C water) expressed in m^3, t = anomaly time (hr), Vca = volume of body of water,

$$\text{EC}_{\text{water}}\ (m^3) = \left(\text{ECw} * \frac{\text{Vol ca}}{10^7}\right) * \frac{t_{anomaly}}{10^{-5}}(hr) \qquad (7)$$

The effect of the anomaly on the body of remaining water would in m^3:

$$\text{Effect}\frac{\text{Enso}}{\text{C}}\text{w} = \text{ECw}\ (m^3) + \text{Evs}\ (m^3) \qquad (8)$$

And in this way obtain,

$$\%\ Water\ Evap\ = \text{Effect}\frac{\text{Enso}}{\text{C}}\text{w} * \frac{100}{Vca} \qquad (9)$$

G. Soil Water Evaporation

Water evaporation from the soil is important in the hydrological cycle due to its thermal regulatory role in the atmosphere and the loss of resources. Conditions assumed for the Evaporation of Water from Soils (Evsoil) and Water Vapor Condensation Temperature follow the pattern of Evaporation of water over bodies of water. The momentum conservation equations are applied to the entire porous medium, and not for each species or phase, in such a way that its result represents the behavior of the environment.

The same references are taken from the analysis of Equations (2) to (5), considering the soil conditions, where σ corresponds to the stress terms, ρ to the density of the porous medium, and g is the acceleration of gravity, at this temperature it is assumed that the amount of water vapor is minimal. Average Nusselt number = 2 * Local Nusselt number. Water vapor pressure above the ground (Pvs), reaches atmospheric pressure at sea level at a pressure of 760 mmHg.

Convection coefficient or surface transmission coefficient (h), quantifies the influence of fluid, surface, and flow properties when heat transfer occurs by convection, which is modeled €with Newton's Law of Cooling: Q=heat transfer by convection (W), h=film coefficient (W/m^2.K), A= Area of the body in contact with the fluid m^2, Ts= body surface temperature (k), T∞= Fluid temperature at a certain distance from the body $Q = h\,.\,A.\,(Ts - T\infty)$ (10).

Convection steam heat transfer coefficient (hv)= 6000 – 15000 W/(m^2 °C)= [1057 - 2641 Btu/(hr-ft^2 °F)]=0.02422(Cal/h. cm^2.°F); Vt= Total volume, Vp= Volume occupied by pores, Vs= Volume occupied by solids, Vw= Volume of water, Va= Volume of air, Ms= Mass of solids, Mw= Mass of water.

$$\text{Water density} = Dw = \frac{Mw}{Vm} = 1\ g/cc \quad (11)$$

$$\text{Actual soil density} = Dr = \frac{Ms}{Vs} 2.65\ g/cc \quad (12)$$

$$\text{Soil porosity} = \phi = \frac{Vp}{Vt} = 1 - \frac{Da}{Dr} \quad (13)$$

It is assumed that the Air Pressure Pa (g/cc) = 254, the water and air temperature Ta, Tg respectively, Soil Density ρs (g/cc) = 2.2; Soil Porosity = 5 (sandy loam soil), Humidity of floor %. The weight of soil solids (g) without pores per unit volume (cc) varies from 1.3 to 1.7 g/cc in sandy soils and from 1.1 to 1.4 g/cc in clay soils, ranges from 2.6 to 2.7 g/cc in most mineral soils averaging 2.65 g/cc textural. The formula can calculate the porosity ϕ of the soil:

$$\text{Porosity} = \phi = 100 - \left(\frac{1-\text{Bulk density Db}}{\text{particle density Dp}}\ x\ 100\right) \quad (14)$$

This process is also governed by the Law of Ideal Gases, which describes the relationship between the pressure, volume, temperature, and quantity (in moles) of an ideal gas so that the amount of water evaporated above the soil (EC water-soil) given in gr/h. m^2, would be:

$$\text{ECw} - \text{s}\left(\frac{\text{gr}}{\text{h}\ m^2}\right) = \text{hp} * \frac{\text{Pvs} - \text{Pv}}{0.082*(\text{Tair}+273)} \quad (15)$$

Where hp= transfer coefficient, water vapor pressure above the ground Pvs=6.28; Vapor pressure Pv(g/cc) =4.42; Air Temp °C. The soil humidity (gr/cc) is taken into account, comparing it with Soil humidity % (data from the region under study)

$$\text{H s}\left(\frac{\text{gr}}{\text{cc}}\right) = \frac{\text{Ds}\left(\frac{\text{kg}}{\text{cc}}\right) x\ \text{Vol.V air \%}}{100}\ x\ 18 \quad (16)$$

E(C water) expressed in m^3, t = anomaly time (hr), Vca = volume of body of water.

$$\text{ECwater} - \text{soil}\ (m^3) = \left(\text{ECwater} - \text{soil}\left(\frac{\text{gr}}{\text{h}\ m^2}\right) * \frac{\text{Vol ca}}{10^7}\right) * \frac{t_{anomaly}}{10^{-5}}\ (hr) \quad (17)$$

The effect of the anomaly on the body of water would remain m^3:

$$Effect\ \frac{\text{ENSO}}{\text{C}}\text{w} = \text{ECw}\ (m^3) + \text{Evs}\ (m^3) \quad (18)$$

And in this way obtain

$$\%\ Evaporated\ Water - soil\ = Effect\ \frac{\text{ENSO}}{\text{C}}\text{w} * \frac{100}{Vca} \quad (19)$$

H. Water vapor in the clouds

Water vapor condensation temperature, assumed conditions: a) between 11 and 25 km altitude the temperature does not depend on the altitude. b) Air as an ideal Gas, Height (h) m=1500, Molecular Weight (M) gr/mol=28.96; Air Temperature °C (To)=100; q vap H2O J/g=2257.104; H2O Vapor Density (kg/m^3) = 0.5977; Po Sea level kPa (J.m) =101 or 760mmHg; g (m/s)=9.81; Density Liq. water (kg/m^3)=958.31; R=0.082; T=anomaly temperature (°C)>38. The following calculations were carried out as follows,

$$dp = Dair - h\ x\ g\ x\ dh \quad (20)$$

Ideal gas then

$$ph = \left(R * \frac{T0}{M}\right) * P(h) \quad (21)$$

$$dp/p = -(\frac{M}{R} * T0)\ dh \quad (22)$$

Thus, after integration

$$p(h) = p(0) * e^{\left(-\frac{h}{h0}\right)} \quad (23)$$

$$ho(km) = R.\frac{To}{M}.g \quad (24)$$

Applying Clausius-Clapeyron Equation

$$\frac{dp}{dt} = \frac{A}{Tevap} \quad (25)$$

$$A\left(\frac{j}{m^3}\right) = q\frac{Vap}{\left(\frac{1}{Dv}\right)-\left(\frac{1}{Dl}\right)} \quad (26)$$

Then combining equations

$$d\ln Tev\ \frac{dp}{A} = -\left(\frac{po}{A} * ho\right) e^{\left(-\frac{h}{h0}\right)} dh \quad (27)$$

$$ln\left(\frac{To}{Th}\right) = \left(\frac{po}{A}\right) * e^{\left(-\frac{h}{h0}\right)} - 1 \quad (28)$$

I. Radius of water droplets in vapor cloud

A drop of water of radius r in equilibrium with its vapor in a cloud, at a given temperature T, with an internal pressure P1 and the vapor around it Pv.

Ec. Laplace $P^o1 - Pv = \frac{2\Upsilon}{r}$ (29)

Ec. Kelvin $Pv = P^o v\ exp\ (2\Upsilon.Vl.\frac{M}{R}.T)$ (30)

Considering air saturated >100% so that the drop can form and rain, drops with r<rc evaporate and when r>rc grow by condensation on the surface of the droplets.), P°v= vapor pressure of the liquid assuming a flat surface (r approx. infinite), Vl = specific volume, M= Weight/molecular mass. It seeks:

a) Represent $Pv = f(r)\Upsilon T = 20\ ^oC$ (31)

b) Estimate the radius of water drops $r = 2\Upsilon.\frac{Vliq}{rt}ln\acute{O}$ (32)

$$r\ (nm) = (2\ .\Upsilon\ .\left(\frac{N}{m}\right)Vl\ \left(\frac{cm3}{g}\right).\frac{\frac{M}{R}*(T+273.25)*LN\left(\frac{Pv}{P^o v}\right)}{100} \quad (33)$$

J. Adiabatic Gradient of the atmosphere

It is assumed that within the control volume, there are adiabatic processes to calculate the Adiabatic Gradient of Air (Y), rescuing the thermodynamic evolution formulated by Clausius (1860).

Applying Clausius-Clapeyron Equation

$$Ln\frac{P}{Po} = (\frac{1}{To} - \frac{1}{T}) \quad (34)$$

$$\frac{\mathrm{dp}}{\mathrm{dt}} = \frac{\mathrm{A}}{\mathrm{T}}\mathrm{evap} \quad (35)$$

$$\mathrm{A} = \mathrm{q}\frac{\mathrm{Vap}}{\left(\frac{1}{\mathrm{Dv}}\right) - \left(\frac{1}{\mathrm{Dl}}\right)} \quad (36)$$

Being A (J/m^3), then combining equations

$$\mathrm{d}\ln \mathrm{Tev} = \frac{\mathrm{dp}}{\mathrm{A}} = -\left(\frac{\mathrm{po}}{\mathrm{A}} * \mathrm{ho}\right) * e^{\left(-\frac{h}{h0}\right)}\, dh \quad (37)$$

$$\ln\left(\frac{\mathrm{To}}{\mathrm{Th}}\right) = \left(\frac{\mathrm{po}}{\mathrm{A}}\right) * \exp - \left(\frac{\mathrm{h}}{\mathrm{ho}}\right) - 1 \quad (38)$$

Below 11km, Using Mayer's Relation and Clapeyron's Equation

$$(\Upsilon) = -\frac{\mathrm{dT}}{\mathrm{dh}} = \mathrm{M}\frac{\mathrm{g}}{\mathrm{Cp}} \quad (39)$$

Variation of pressure as a function of height

$$\left(\frac{\mathrm{P}}{\mathrm{Po}}\right) = \left(1 - \Upsilon.\frac{\mathrm{h}}{\mathrm{To}}\right)\mathrm{e}^{\left(\frac{cp}{R}\right)} \quad (40)$$

With the help of an optimization tool (DECASAI) in MS. EXCEL®, the °F and °C values are obtained that minimize the relative errors of both the saturation pressures along the Calculations applying the equations (2)-(40).

K. Thermodynamics as an Unbalanced System

For this study outside of equilibrium, the Onsager relations are proposed, as they are closely connected with the detailed equilibrium principle and followed by the linear approximation near equilibrium. Consider new variables defining the gradients or thermodynamic forces and the flux densities that are dual to the forces of the quantities specified in the Onsager reciprocity relations. From the above, it is obtained that:

$$\sigma = \sum_i J_{ij}\frac{\partial F_i}{\partial X_i}\frac{\partial F_j}{\partial X_j} \quad (41)$$

Where: σ = entropy creation rate, Jij= small flows, Fi, Fj= thermodynamic forces (very slowly), linearly related to the flows, and associated with the gradient of the forces, parameterized by a symmetric matrix of positive coefficients denoted by L, known as the Onsager reciprocity relationship.

IV. RESULTS

A. CASE STUDY: Analysis of the Meteorological Event Related to the 2017 Drought in Guri Dam-Venezuela

In this case, the largest dam in the country for generating electrical energy strongly depends on the water basins of the south, such as the Caroní River and Caura. El Niño is the reason for understanding the phenomenon itself analyzed from the thermodynamic and transport phenomena point of view. Between 2016 and 2017, The Niño anomaly caused damage to the hydroelectric generation of the country Venezuela. For the application of the model, the following parameters and values are taken (see Table 2).

Table 2. Thermodynamic variables of the system.

Symbol	Description	Unit	Values	Symbol	Description	Unit	Values
Tg	Air Temperature	℃	35	H	Local Soil Moisture	%	0.126
Ta	Water Temperature	℃	27	Vv	Wind speed	*Km/h*	8
Te	Temperature Anomaly (Enos)	℃	38	h	Reference Atmospheric Height	*mm Hg*	1500
p	Atmospheric pressure	*Kpa*	101	L	Long Course for the Wind	*cm*	100
		Atm	1	A	Body of Water Area	Km^2	3990
		mm Hg	760	Vol	Water Volume of the body of water	m^3	$1{,}10^8$
Pva	Water/Soil Vapor Pressure	*mm Hg*	6,28	A	Biodiverse Area	Km^2	5.77^{11}
Vl	Specific Liquid Volume	*cc/g*	1.042	Q	Water Flow Biodiverse Area	m^3/s	4000
Vl	Specific Liquid Volume	cc/mol	18	t	Anomaly Duration (Enso)	*months*	4
r	Local Radiation	W/m^3	1387				

Source: Author.

As a result of the model application, the following results were obtained, as shown in Table 3.

Table 3. Results of the DECASAI Model applied in Gurí Dam-Venezuela.

Parameters	Unit	Results	Parameters	Unit	Results
Water Removal/Body of Water	g/h m^2	19,01	Relative Humidity Air	%	83.33
Water/Soil Removal	g/h m^2	31.73	Activation Energy for Droplet Formation	$J * 10^{-18}$	20.27
Temperature Steam Water Clouds	°C	96.19	Entropy	Cal/mol	17.346
Circuit Temperature Convective Mixture Enso	°C	22.16	Final Soil Moisture	gr/h. m^3	2.18
Ambient Temperature Mixing at Height	°C	7.4	The volume of Water Removed Body of water	m^3	21.846.482
Estimated Soil Temperature	°C	32.6	Volume of Water Removed Biodiversity	m^3	52.731.393
Drop Radius	nm	9.24	% Water Removed(+)	%	30.18
Critical Drop Radio	nm	4.60			

Source: Author

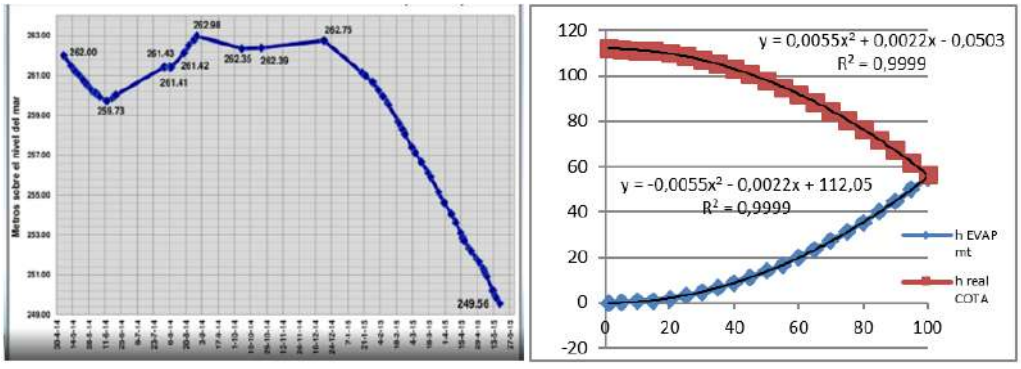

(a) (b)

Fig. 6. Guri Reservoir (a) Guri Reservoir Level Identification Curve 2015 (msnm), (b) Amount of water removed in the Guri Reservoir (blue) and Perception of the flow Q of the reservoir. Source: Author.

CONCLUSIONS

1. The developed model, based on the approach of deductive analysis, allowed the understanding from a thermokinetic point of view of the behavior and possible forecast of the dynamic conditions of the soil-atmosphere, during the occurrence of atmospheric anomalies.
2. The model allows the assessment of the effects on the meteorological, agricultural, hydrological, and social vulnerabilities and manages the water resources of the studied microclimates, located within the Hadley cells, considered as a control volume.
3. Because the evaporation itself is subject to various atmospheric processes, including solar radiation and turbulence processes, the inclusion of these processes required considering a control volume that covered an important fraction of the soil and at its time a strip of up to eleven kilometers of the atmosphere.
4. Due to the previous conclusion, the mass, momentum, and energy conservation equations were considered, and applied to the lower atmosphere and specifically to the atmospheric boundary layer, considering the soil-water water removal equations, since these allow the evaporation process, in which DECASAI model works.

RECOGNITIONS

Recognition is given to Universidad Nacional Experimental Politecnica UNEXPO, Vicerrectorado Puerto Ordaz, for its outstanding work in the training of engineers who wish to generate knowledge of science and for science. As well as the invaluable commitment and dedication of Dr Oscar Dam G., for its academic contributions and the processing of the obtained results.

REFERENCES

[1] P. Eagleson, "Climate, soil, and vegetation: 1. Introduction to water balance dynamics.," *Water Resources Research,* vol. 14, no. 5, pp. 705-712., (1978b).

[2] J. Shukla and Y. Mintz, "Influence of land-surface evapotranspiration on the earth's climate.," *Science,* vol. 215, no. Crossref, Google Scholar, p. 1498–1501, 1982.

[3] D. Entekhabi, I. Rodriguez-Iturbe, and Bras, "Variability in large-scale water balance with land surface-atmosphere interaction. " *J. Climate,* no. 5, p. 798–813, 1992.

[4] R. D. Koster, P. A. Dirmeyer and A. N. Hahmann, "Comparing the degree of land–atmosphere interaction in four atmospheric general circulation models," *J. Hydrometeor,* no. 3, p. 363–375, 2002.

[5] A. Numaguti, "Dynamics and energy balance of the Hadley circulation and the tropical precipitation zones: Significance of the distribution of evaporation.," *J. Atmos. Sci,* vol. 50, no. Link, Google Scholar, p. 1874–1887, 1993.

[6] P. C. D. Milly and A. B. Shmakin, "Global modeling of land water and energy balances. Part I: The Land Dynamics (LaD) model," *J. Hydrometeor,* vol. 3, no. Link, Google Scholar, p. 283–299, 2002.

[7] P. M. Cox, R. A. Betts, C. B. Bunton, R. L. H. Essery, P. R. Rowntree, and J. Smith, "The impact of new land surface physics on the GCM simulation of climate and climate sensitivity," *Climate Dyn,* vol. 15, no. Crossref, Google Scholar, p. 183–203, 1999.

[8] V. D. Pope, M. L. Gallani, P. R. Rowntree and R. A. Stratton, "The impact of new physical parameterizations in the Hadley Centre climate model: HadAM3," *Climate Dyn,* vol. 16, no. Crossref, Google Scholar, p. 123–146, 2000.

[9] J. Polcher and Coauthors, "A proposal for a general interface between land surface schemes and general circulation models," *Global Planet. Change,* vol. 19, p. 261–276, 1998.

[10] J. Bjerknes, "A possible response of the atmospheric Hadley circulation to equatorial anomalies of ocean temperature.," *Tellus,* vol. 18, pp. 820-829, 1966.

[11] D. R. Pozo, D. Martínez and C. Madeyvis, "Simulación numérica tridimensional de una celda convectiva simple en condiciones tropicales utilizando el modelo ARPS," *Revista Cubana de Meteorología,* vol. 8, no. 1, 2001.

[12] H. Romero , P. Smith, M. Mendonça and M. & Méndez, "Macro y mesoclimas del altiplano andino y desierto de Atacama: desafíos y estrategias de adaptación social ante su variabilidad."," *Revista de Geografía Norte Grande,* no. 55, pp. 19-41, 2013.

[13] A. h. Oort and J. J. y Yienger, "Variabilidad interanual observada en la circulación de Hadley y su conexión con ENOS," in *Diario del Clima*, 1996, pp. 2751-2767.

[14] M. T. Landahl, "A wave-guide model for turbulent shear flow," *Journal of Fluid Mechanics,* vol. 29, no. 3, pp. 441-459, 1967.

[15] A. D. D. Craik, "Wind-generated waves in thin liquid films," *Journal of Fluid Mechanics,* vol. 26, no. 2, pp. 369-392, 1966.

[16] J. W. Miles, "On the generation of surface waves by shear flows—part 4," *J. Fluid Mech,* no. 13, p. 433–448, 1962.

[17] G. R. Meindertsma, "Design and effectiveness of a novel tripping device for wind tunnel testing.," *University OF Twente.(Tesis Doctoral),* 2020.

[18] H. Schlichting, Boundary Layer Theory, McGraw-Hill, Inc, 7th edition, 1979.

[19] M. S. Genç, I. Karasu and H. H. Açikel, "Un estudio experimental sobre la aerodinámica de Perfil aerodinámico NACA2415 a números Re bajos," *ciencia experimental térmica y de fluidos,* 2012.

[20] O. Dam, "Toma de Decisones en Ciencias e Ingenieria," in *III Congreso Latinoamericano de Ciencias, Tecnologia e Innovacion*, Quito, Ecuador, 2020.

Mara Girón, MSc. Industrial Engineer, Venezuelan. Student of the Doctorate of Engineering Sciences at UNEXPO vice-rector Puerto Ordaz.

ISSN-e: 2737-6419

Athenea Journal
Vol.4, Issue 14, (pp. 45-52)

https://doi.org/10.47460/athenea.v4i14.67

Caracterización de la resistencia a compresión del adobe tradicional con adición de zeolita

Feijoo Calle Ernesto Patricio
https://orcid.org/0000-0001-6901-7933
pfeijoo@uazuay.edu.ec
Universidad del Azuay
Cuenca-Ecuador

Feijoo Guevara Bernardo Andrés
https://orcid.org/0000-0002-1089-1332
bernardofeijoo@uazuay.edu.ec
Universidad del Azuay
Cuenca-Ecuador

Núñez Rodas Leonardo Aníbal
https://orcid.org/0000-0003-4730-6114
lnunez@uazuay.edu.ec
Universidad del Azuay
Cuenca-Ecuador

Recibido (20/08/2023), Aceptado (23/11/2023)

Resumen: Este trabajo tuvo como objetivo principal, valorar la resistencia a compresión del adobe tradicional y además del adobe con adición de zeolita, como complemento de la arcilla, para de esta forma prolongar la vida útil de los yacimientos sedimentarios arcillosos presentes en la zona y así potencializar nuevos depósitos de zeolita. Se inició el trabajo con la elaboración de probetas con dimensiones específicas, para el adobe tradicional y también para adobe con porcentajes complementarios de zeolita, en el orden del 25 % y 50 %. Para valorar la resistencia a la compresión de estos elementos, se confeccionaron 12 probetas de cada uno de los grupos, probetas con dimensiones aproximadas de 5x5x10 cm., y se sometieron al ensayo respectivo, con el equipo adecuado. Los resultados presentan valores que se deben tomar en consideración y se concluye con recomendaciones que pueden coadyuvar para el mejoramiento de ciertos aspectos de los elementos estudiados.

Palabras clave: adobe, arcilla, compresión, zeolita.

Characterization of traditional adobe with addition of zeolite regarding compressive strength

Abstract. - This work aimed to assess the compressive strength of traditional adobe and adobe by adding zeolite as a complement to clay to prolong the useful life of the clayey sedimentary deposits in the area and thus potentiate new zeolite deposits. The work began with elaborating test tubes with specific dimensions for traditional adobe and adobe with complementary percentages of zeolite in 25% and 50%. To assess the compressive strength of these elements, 12 test tubes from each of the groups were made, test tubes with approximate dimensions of 5x5x10 cm, and they were subjected to the respective test with the appropriate equipment. The results present values that must be considered and concluded with recommendations to help improve certain aspects of the studied elements.

Keywords: Adobe, clay, compression, zeolite.

I. INTRODUCCIÓN

La tierra es sin dudas el material de construcción más antiguo de los empleados por el hombre en su evolución histórica. Paradójicamente, ha llegado hasta el presente constituyendo prácticamente la única alternativa para que una parte significativa de la humanidad pueda disponer de una vivienda en condiciones mínimas de habitabilidad [1]. El adobe es un material muy usado en las construcciones más antiguas, ya que hoy en día por lo general es común ver el uso de ladrillos y concreto, sin embargo, aún hoy vemos este tipo de construcciones en adobe que comúnmente se mezclan con otros tipos de materiales y mampostería Es común que en los sistemas constructivos de las construcciones en tierra se presentan mezclas de diferentes tipos de mampostería: mampuestos en sillares de piedra y/o tapiales, y/o muros en adobe [2]. El adobe es un tipo de mampostería artesanal muy simple, compuesto por tierra, paja y agua. Para su elaboración, primero se elige una zona cercana al lugar de construcción, de donde se extraerá la tierra, luego se combina con paja y agua hasta lograr una mezcla uniforme y maleable. Por último, la mezcla es colocada en moldes de madera para crear las piezas de adobe y posteriormente se dejan secar al aire libre de 30 días a 60 días [3].

A lo largo de la historia la transformación de los suelos naturales en materiales constructivos ha tenido diferentes procedimientos, derivados de los recursos naturales locales, de las condicionantes medioambientales y de procesos de ensayo y error ancestrales. La mayor parte de las comunidades que emplearon la tierra para edificar se dio cuenta de que era posible mejorar sus condiciones originales a partir de la interacción de dos factores: la humedad y la densidad [4].

La mampostería como sistema constructivo presenta según su disposición y trabado distintas propiedades mecánicas en función de la dirección de las cargas soportadas, es decir, su comportamiento no es estrictamente isótropo ni homogéneo debido a que las juntas de unión establecen planos débiles de rigidez. Sin embargo, en el presente artículo, la mampostería de adobe es tratada como un medio continuo y homogéneo para la obtención de sus propiedades desde un punto de vista macro mecánico [5].

El adobe generalmente debe tener mayor porcentaje de arena que arcilla. Estos, en su comienzo, eran confeccionados a mano, y luego se utilizaban moldes para lograr una mayor producción. La tierra debe permanecer húmeda durante dos días, para fermentarla y lograr que los aglomerantes actúen. Para elaborar el adobe, el barro se arroja dentro del molde humedecido, luego se comprime con la mano o los pies, repartiendo uniformemente el material; posteriormente se engrasa la superficie, y se desmolda cuidadosamente para que las aristas permanezcan en buen estado [6]. Las arcillas de baja calidad se encuentran disponibles en casi cualquier parte; como resultado de esto, por ejemplo, la manufactura de ladrillos de construcción y de baldosas que no requieran propiedades especiales son de fabricación local, para las cuales la beneficiación intensa de la materia prima no es una prioridad [7].

Las pruebas experimentales de los procedimientos de construcción de las piezas de adobe, probetas, especificaciones de ensayo, análisis de resultados y caracterización de las principales propiedades mecánicas del adobe como son módulo de elasticidad, resistencia a la compresión, cortante y flexión; fueron realizadas debido a la necesidad primordial de una norma, pues actualmente no existe, para realizar los ensayos en este tipo de material [3]. A más de lo expuesto, también es muy importante conocer la resistencia a fuerzas que posee el adobe, en este caso se los caracterizó mediante pruebas a la compresión, es decir se determinó la resistencia a la compresión simple (RCS) de probetas. La RCS se define como su capacidad para resistir esfuerzos y fuerzas aplicadas adquiriendo deformaciones sin llegar a romperse.

Se dice que cuando una fuerza actúa sobre un cuerpo, se presentan fuerzas resistentes en las fibras del cuerpo que se denominan fuerzas internas. Fuerza interna es la resistencia interior de un cuerpo a una fuerza externa. Así que cuando se usa el término esfuerzo, se refiere a la magnitud de la fuerza por unidad de área. De tal forma, que la resistencia de un material es la propiedad que tiene para resistir la acción de las fuerzas. El esfuerzo de compresión es una presión que tiende a causar una reducción de volumen [8]. La máquina de ensayos tiene como función comprobar la resistencia de diversos tipos de materiales, para esto posee un sistema que aplica cargas controladas sobre una probeta (modelo de dimensiones preestablecidas) y mide en forma gráfica la deformación, y la carga al momento de su ruptura [9]. Cabe indicar que las muestras de los diferentes materiales y sus propiedades pueden variar según el grado de cementación o variaciones en la composición mineralógica [10].

En teoría, para mejorar la resistencia a la compresión del adobe y debido a la presencia de importantes depósitos en la región, se propone la adición de zeolita en la elaboración del adobe tradicional. Esta adición sustituye en cantidades considerables a la arcilla, lo cual aumenta la vida útil de los yacimientos de arcilla actuales. Según Costafreda [11], las mezclas a base de zeolitas fueron las más eficientes, ya que aumentaron la resistencia a compresión como sustitución del cemento, pero en este estudio se utilizará este mineral como sustituto de arcilla.

Este trabajo propone, a partir de la base teórica utilizada para tal fin, la metodología para la obtención de los objetivos propuestos, describiendo un procedimiento claro y estadístico, que puede ser utilizado en otros casos, generando una estrategia para obtener los instrumentos de evaluación adecuados; Cabe recalcar que en este trabajo los resultados obtenidos han generado una expectativa muy importante sobre su aplicación.

II. MATERIALES Y MÉTODOS

Para desarrollar esta propuesta, se elaboraron un total de 36 muestras (probetas) de adobe, todas con las mismas dimensiones aproximadamente, para lo cual se utilizó un molde de forma de paralelepípedo de 5 cm x 5 cm x 10 cm y de esta forma tratar de que las probetas tengan un tamaño homogéneo. Estas dimensiones de probetas son las que se utilizan generalmente para los ensayos de resistencia a compresión. Ahora las 36 probetas se dividieron en 3 grupos. Las primeras 12 son exclusivamente probetas de adobe tradicional, las segundas 12 son probetas con una adición de 25 % de zeolita en lugar de arcilla y las ultimas 12 con adición del 50 % de zeolita en lugar de arcilla. La cantidad de probetas de cada grupo supera las 4 recomendadas en la teoría.

El tipo de zeolita utilizada fue la clinoptilolita perteneciente al grupo de la heulandita, cuyas características físicas son: Granulometría 40%, máximo retenido en malla 100, color marrón – verdoso, pH 9.8 y humedad 7 % máx.

El procedimiento para la elaboración de las probetas fue diluir la cantidad de zeolita en sus diferentes porcentajes con agua hasta que se convierta en un fluido manejable y con ello poder mezclarlo con arcilla, logrando así una mezcla homogénea, a través de una mezcladora tipo celda Denver. Al adicionar la zeolita en las diferentes muestras se ingresa en los moldes preestablecidos se desmolda y se los deja secar 4 semanas, específicamente 28 días al aire libre, como se procede con el adobe tradicional.

Algunas probetas se las puede observar en la figura 1.

Fig. 1: Probetas de adobe.

Luego de obtener las diferentes probetas, las mismas fueron sometidas al ensayo de carga, mediante una prensa marca Humboldt, el cual proporciona las garantías para la obtención de la resistencia a la compresión de los elementos sometidos. Este equipo se lo puede observar en la figura 2.

Fig. 2: Prensa Humboldt para ensayos de compresión.

The boundary layer displacement thickness $\delta*$, which quantification is not considered in this work, is given by:

$$\delta*(x) = 1.72x\sqrt{Rex} \quad (1)$$

The boundary conditions can be applied for flow over a flat plate, considering the soil surface layer of -5cm to 10cm above and establishing standardized soil porosity values.

III. RESULTADOS

Los resultados de los ensayos de resistencia a la compresión se presentan a continuación, en las tablas 1, 2 y 3. Los resultados se muestran en mega pascales.

En la tabla 1 se presentan los resultados de la resistencia a la comprensión del adobe tradicional, cuyos valores varían entre 1.15 MPa y 1.61 MPa, con un promedio de 1.41 MPa, una mediana de 1.47 MPa y desviación estándar de 0.17.

Tabla 1: Resultados de resistencia a compresión del adobe tradicional.

Probetas A	RCS (MPa)
1	1.15
2	1.49
3	1.46
4	1.15
5	1.17
6	1.55
7	1.59
8	1.61
9	1.45
10	1.29
11	1.50
12	1.51

Los resultados para el adobe tradicional se los puede observar en la figura 3.

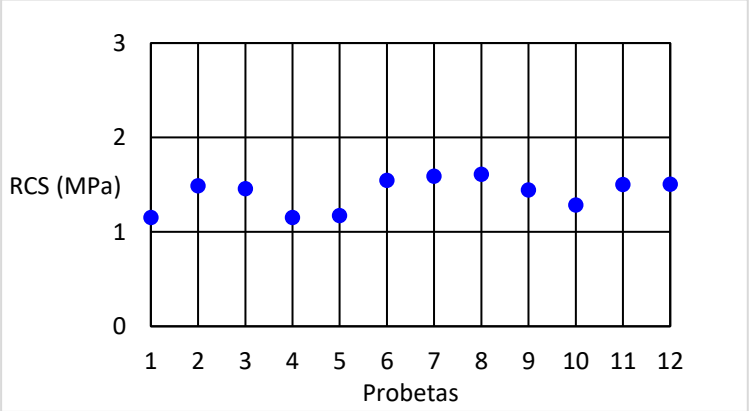

Fig. 3: Resultados de resistencia a compresión del adobe tradicional.

Para el segundo grupo de probetas, las que contuvieron un 25 % de zeolita, los resultados varían desde 1.18 MPa hasta 1.72 MPa, con un promedio de 1.41 MPa, mediana de 1.36 MPa y desviación estándar de 0.19, los resultados se los puede observar en la tabla 2.

Tabla 2: Resultados de resistencia a compresión del adobe con 25 % de zeolita.

Probetas B	RCS (MPa)
1	1.31
2	1.43
3	1.30
4	1.42
5	1.20
6	1.60
7	1.72
8	1.70
9	1.18
10	1.26
11	1.27
12	1.58

Los resultados los puede observar en la figura 4.

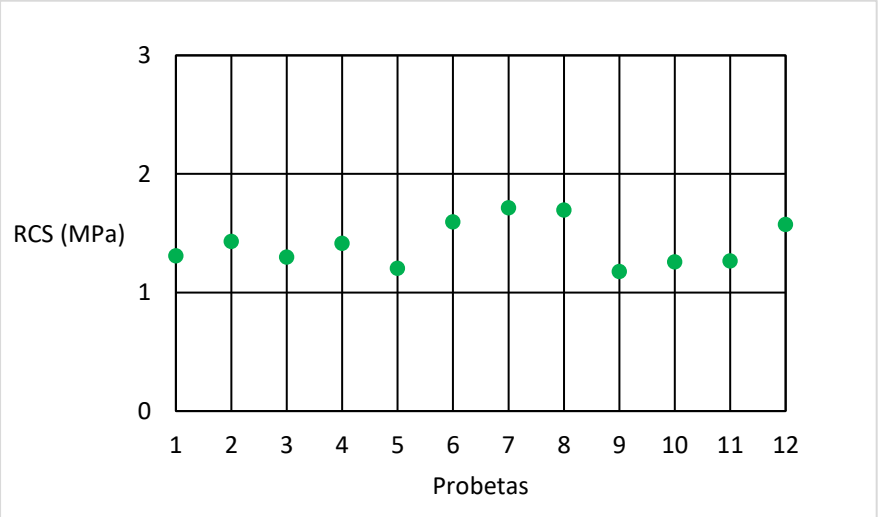

Fig. 4: Resultados de resistencia a compresión del adobe con adición de zeolita al 25 %.

Finalmente se ejecutaron los ensayos para las probetas de adobe con adición de zeolita al 50% y los resultados para la resistencia a compresión varían desde los 0.77 MPa hasta 1.16 MPa, promedio de 0.97 MPa, mediana de 0.97 MPa y desviación estándar de 0.12, los resultados se presentan en la tabla 3.

Tabla 3: Resultados de resistencia a compresión del adobe con 50 % de zeolita.

Probetas C	RCS (MPa)
1	0.97
2	0.95
3	0.88
4	1.07
5	0.77
6	0.80
7	1.13
8	0.97
9	0.96
10	0.97
11	1.07
12	1.16

Los resultados se los puede observar en la figura 5.

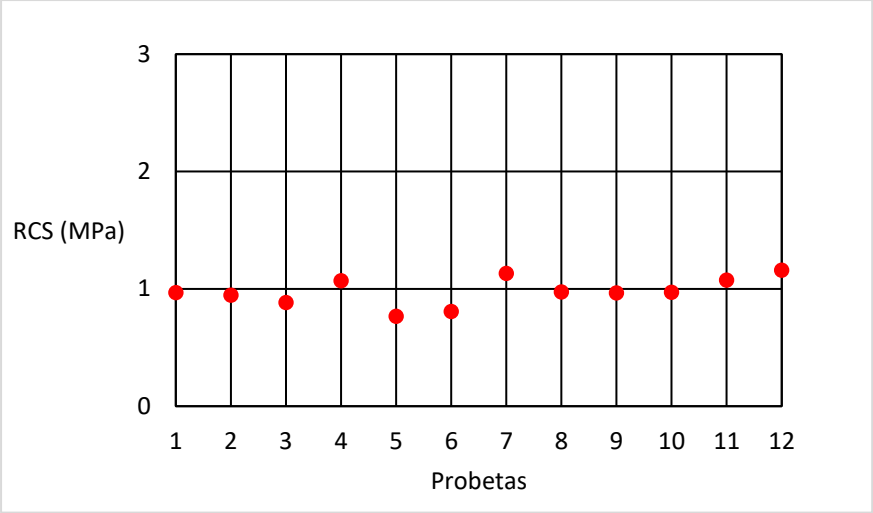

Fig. 5: Resultados de resistencia a compresión del adobe con adición de zeolita al 50 %.

Una compilación de los resultados, media, mediana y desviación estándar se muestran en la tabla 4.

Tabla 4: Análisis de los valores de los grupos de probetas.

	Media (MPa)	Mediana (MPa)	Desviación Estándar
Adobe tradicional	1.41	1.47	0.17
Adobe con 25 % de zeolita	1.41	1.36	0.19
Adobe con 50 % de zeolita	0.97	0.97	0.12

CONCLUSIONES

- La añadidura de zeolita, para complementar el uso de arcilla, nos permite determinar que los elementos evaluados, en el caso de adición de 25%, mantiene la resistencia a la compresión de las probetas elaboradas, cuyo valor está en el orden de 1.4 MPa.
- Cabe indicar que los datos del adobe con adición del 50 % de zeolita, presentan una menor dispersión, pero tienen disminución en la resistencia a la compresión. La desviación estándar del adobe con adición del 25 % de zeolita es mayor, pero no existe variación en la resistencia a la compresión comparada con el adobe tradicional.
- Los adobes elaborados con adición de zeolita pueden ser usados como elementos ornamentales, debido a que su resistencia a la compresión no es muy alta, pero si mantendrían durabilidad en el tiempo y al mismo tiempo permiten una excelente maniobrabilidad. Además, la viabilidad económica del uso de zeolita es bastante aceptable debido a su bajo costo.
- Este trabajo presenta una metodología de trabajo simple y sencilla, para la caracterización de los elementos estudiados, por lo que su puesta a punto debe profundizarse con un mayor número de probetas y de esta forma el proceso sea avalado.

REFERENCIAS

[1] J. Toirac Corral, "El suelo-cemento como material de construcción", Revista Ciencia y Sociedad, vol. XXXIII, núm. 4, pp. 520-571, 2008.
[2] M. Díaz-Torres, H. Parada-Carrillo, y M. Alvarado-Arias, "Usos del adobe en diferentes países de América Latina", Revista Sostenibilidad, Tecnología y Humanismo, vol. 10, núm. 2, pp. 73-81, 2019. https://doi.org/10.25213/2216-1872.22.

[3] P. Catalán Quiroz, J. Y. Moreno-Martínez, A. Galván, y R. Arroyo Matus, "Obtención de las propiedades mecánicas de la mampostería de adobe mediante ensayes de laboratorio", Acta Universitaria, vol. 29, pp. 1–13, 2019. https://doi.org/10.15174/au.2019.1861.
[4] L. F. Guerrero Baca, "El uso de tierra modelada en la intervención de componentes constructivos de adobe", Intervención, vol. 2, núm. 22, pp. 131–187, 2020.
https://doi.org/10.30763/intervencion.236.v2n22.15.2020.
[5] J. D. Rodríguez-Mariscal y M. Solís, "Hacia una metodología para la caracterización experimental del comportamiento a compresión de la mampostería de adobe", infconstr, vol. 72, núm. 557, pp. e332, 2020.
https://doi.org/10.3989/ic.67456.
[6] A. Doria, J. Orozco. "Evaluación de propiedades físico-químicas y mecánicas del adobe elaborado con cal para su uso en la construcción sostenible". Revista Colombiana de Tecnologías de Avanzada, vol. 1, núm. 35, pp. 89 – 94, 2020.
[7] R. Uribe. "Investigaciones de materias primas minerales no metálicas en el Ecuador". Revista Politécnica, vol. 36, núm. 3, pp. 34 – 44, 2015.
[8] J. Nureña. "Influencia del estabilizante de cemento y tipos de suelos sobre la resistencia y durabilidad de un adobe constructivo". Trujillo. Universidad Privada del Norte. Perú. 2017.
[9] P. Feijoo, A. Flores, B. Feijoo, "The Concept of the Granulometric Area and Its Relation with the Resistance to the Simple Compression of Rocks", presentado en la 7th International Engineering, Sciences and Technology Conference (IESTEC), Panamá, Panamá, 2019, pp. 52-56, doi: 10.1109/IESTEC46403.2019.00018.
[10] P. Feijoo, J. Padrón. "La Resistividad de Rocas y su Relación con la Resistencia a Comprensión Simple en Mina". UCT, vol. 24, núm. 99, pp. 61-67. 2020.
[11] Costafreda Mustelier, J. L., Sánchez, M., Costafreda Velázquez, J. L. "Las zeolitas naturales de Iberoamérica". Fundación Gómez Pardo, Madrid. 2018. ISBN 978-84-09-00125-5.

LOS AUTORES

Patricio Feijoo Calle, Ingeniero en Minas, graduado en la Universidad del Azuay (Cuenca-Ecuador), con estudios y pasantías en: Bolivia, Brasil, España, Australia en áreas de la geología, geofísica y desarrollo de actividades de explotación de minas. Se encuentra vinculado a la docencia en la Universidad del Azuay.

Bernardo Feijoo Guevara, Ingeniero Civil, por la Universidad del Azuay (Cuenca-Ecuador), con estudios y pasantías en: Colombia, Perú, Cuba y Panamá, en áreas de caracterización de materiales y procesos de elaboración de cementos y hormigones. Está vinculado a la docencia e investigación en la Universidad del Azuay.

Leonardo Núñez Rodas, Ingeniero en Minas, graduado en la Universidad Central del Ecuador (Quito - Ecuador), con estudios y pasantías en: Ecuador, Chile, Bolivia, Brasil y Colombia en las áreas de la investigación geológica, explotación minera, procesos metalúrgicos y gestión ambiental. Se encuentra vinculado a la docencia en la Universidad del Azuay, mantiene actualmente el cargo de Profesor Titular e Investigador.

ISSN-e: 2737-6419

Athenea Journal
Vol.4, Issue 14, (pp. 53-62)

https://doi.org/10.47460/athenea.v4i14.68

La inteligencia artificial y su aporte en la optimización de la logística empresarial

Pulido Talero William Eduardo
https://orcid.org/0000-0003-4813-8087
Grupo de Investigación CEIL-MD centro de estudios Industriales y logísticos para la productividad año 2015.
Corporación Universitaria Minuto de Dios
Bogotá – Colombia

Castañeda Jerez Carlos Eduardo
https://orcid.org/0000-0001-7779-0838
Grupo de Investigación CEIL-MD centro de estudios Industriales y logísticos para la productividad año 2015.
Corporación Universitaria Minuto de Dios
Bogotá – Colombia

Recibido (10/08/2023), Aceptado (13/11/2023)

Resumen: El inminente arribo de la inteligencia Artificial plantea más interrogantes que certezas; uno de los cuales tiene que ver con la prodigalidad de usos y finalidades que esta tecnología puede tener en el ámbito de la logística. Las investigaciones que profundizan en torno a la aplicación de la IA en determinados escenarios han revelado su utilidad para apoyar procedimientos en laboratorios clínicos para vaciar de productividad y eficiencia las economías agrarias, y para los efectos de este trabajo, la IA se ha extendido a la interioridad de las fábricas, las bodegas, las cadenas de ensamblaje y suministro, brindándole facilidades a las empresas en gestión del tiempo y en la predicción de tendencias de consumo. La presente investigación tuvo como propósito auscultar los beneficios y utilidades que se desprenden de la implementación de la IA en las actividades logísticas de las empresas. Se usa el método deductivo, la técnica de análisis documental sobre fuentes secundarias, y es de tipo descriptivo. Los resultados están orientados a los análisis de sus efectos en las cadenas de suministro.

Palabras clave: Inteligencia, logística, eficiencia, optimización.

Artificial intelligence and its contribution to business logistics optimization

Abstract. - The imminent arrival of Artificial Intelligence raises more questions than certainties; one of which has to do with the prodigality of uses and purposes that this technology can have in the field of logistics. Research that delves into the application of AI in certain scenarios has revealed its usefulness in supporting procedures in clinical laboratories to deplete agricultural economies of productivity and efficiency, and for the purposes of this article, AI has been extended to the interior of factories, warehouses, assembly and supply chains, providing companies with facilities in time management and in predicting consumption trends. The purpose of this research was to explore the benefits and utilities that arise from the implementation of AI in the logistics activities of companies. It uses the deductive method, the documentary analysis technique on secondary sources, and is descriptive, the results are oriented towards the analysis of its effects on supply chains.

Keywords: Intelligence, Logistics, Efficiency, Optimization.

I. INTRODUCCIÓN

Los procesos manuales en las empresas de actual tiempo están cediendo ante la cada vez más extendida proliferación de herramientas de IA, lo que obliga a preguntar tal como lo hacen Garay y Candia [1] acerca de sí las máquinas reemplazaran al ser humano. Obviando la fatalidad de las consecuencias totales de la anterior afirmación, es cierto que la IA destaca por la realización de actividades de manera más precisa y eficiente comparada con cualquier persona. En este sentido, el objetivo del trabajo está orientado a poder hacer un análisis muy sencillo de lo que significa en logística empresarial y en los sistemas de cadenas de suministro, la incorporación de herramientas y metodologías orientadas por medio de la inteligencia artificial. Ello aplicado a la logística, ha contribuido al menos en tres aspectos: en la predicción de tendencias de consumo, en la automatización del traslado de productos, en el almacén y en la selección de rutas de transporte ofreciendo desplazamientos más eficientes, como lo indica Mora [2]. Otros investigadores como Giraldo [3], Escudero Serrano [4] y O´Brien [5] también rescatan ventajas en la aplicación de la IA en los procesos logísticos. Es menester auscultar los beneficios y utilidades de esta tecnología a razón de lo explicado por los citados investigadores.

Lo anterior afirma la relevancia de la IA, sin que se desconozca la contribución de los demás investigadores, que le han seguido la pista a la implementación de la IA en otros ámbitos científicos, y productivos. La primera sección de este documento está referida a la IA como conceptos y aplicaciones, para cerrar con la adecuación de los escenarios logísticos a las nuevas realidades tecnológicas como lo plantea Álvarez [6]. Por otra parte, la hipótesis destaca los alcances de la IA en toda la organización logística abocados a imprimir celeridad, eficiencia y optimización en las tareas y procesos empresariales, así lo expresa González García y otros [7]. La segunda parte de este trabajo está basada en la IA aplicado al campo de la logística: beneficios y recomendaciones. La tercera parte es la metodología con la que se ha realizado este trabajo. La cuarta sección son los resultados y la última sección las conclusiones y finalizando con las referencias bibliográficas.

II. LA IA COMO CONCEPTO Y APLICATIVO DE DIVERSOS ÁMBITOS CIENTÍFICOS Y PRODUCTIVOS

Ponce Gallegos y otros [8] aducen que la IA es un ámbito de la ciencia de gran interés por ser un área multidisciplinaria donde se realizan sistemas que tratan de hacer tareas y resolver problemas como lo hace un humano, así mismo se trata de simular de manera artificial las formas del pensamiento y cómo trabaja el cerebro para tomar decisiones, por su parte, las Redes Neuronales son un paradigma de aprendizaje y procesamiento automático inspirado en la forma en que funciona el cerebro para realizar las tareas de pensar y tomar decisiones (sistema nervioso). En este contexto, el cerebro consiste en un sistema de interconexión de neuronas en una red que colabora para producir un estímulo de salida, así lo indica Ponce Gallegos y otros [8]. En la definición anterior es ostensible la simplificación y sistematización de aquellas acciones realizadas por el ser humano, ahora replicadas por la inteligencia artificial. En el campo de la medicina, por ejemplo, Herrera Triguero y otros [9] resaltan la valiosa integración entre el Big data y la inteligencia artificial. Los autores argumentan que la integración de estas tecnologías puede mejorar la eficiencia y la calidad de los servicios de laboratorio, así como proporcionar una mejor atención médica a los pacientes.

En la figura 1 se observa cómo se da una doble vía entre la captura de datos por medio de hardware, redes conectadas, infraestructura y centro de datos, pasando por el procesamiento de datos en segundo paso, donde se tiene el uso de tecnologías. Luego se realiza el análisis de datos por medio de la analítica, predicción y servicios en la nube. Luego se tiene la ejecución de datos como servicios e integración y todo el tema de vendedores de software. Se observa cómo se puede dar el proceso en doble vía.

Fig. 1. Esquema del proceso de conversión de datos a información.

Además, aparecen otros nuevos conceptos menos populares y más difíciles de entender, pero también muy conocidos y con un rol cada vez más creciente, como son: el IoT y el Machine Learning. Estos conceptos complementan muy bien el Big Data y la Inteligencia Artificial ya que utilizan el registro de los datos obtenidos que son clasificados, gestionados y analizados posteriormente para conectar máquinas entre sí y realizar modelos predictivos, entre otros usos así lo hace conocer Cardenes [10].

La investigación de los citados autores describe cómo la tecnología del Big Data puede ayudar en el análisis de grandes conjuntos de datos generados por los servicios de laboratorio, proporcionando información valiosa para la toma de decisiones clínicas y mejorando la precisión del diagnóstico. [11]. Además, la IA puede ser utilizada para desarrollar modelos predictivos que ayuden a identificar patologías y mejorar la precisión del diagnóstico y el pronóstico afirmado por Cardenes [10]. Los autores también destacan que la integración de estas tecnologías puede mejorar la eficiencia de los servicios de laboratorio, reduciendo el tiempo necesario para obtener resultados y mejorando la productividad de los profesionales de laboratorio. Además, la integración de la tecnología también puede mejorar la seguridad y la calidad de los resultados, ya que los sistemas automatizados pueden reducir la posibilidad de errores humanos descrito por Minnetti y otros [12].

La IA también ha rendido sus frutos trasladada a procesos productivos en las economías agrarias; la investigación de Palomo Zurdo y González Sánchez [13] explora cómo el vector de la digitalización de los fondos de recuperación puede impactar en la economía social. Su trabajo explora también cómo la digitalización puede mejorar la eficiencia y la productividad de las organizaciones de economía social, y cómo esto puede contribuir a su crecimiento y sostenibilidad. Los autores advierten que la digitalización puede mejorar la gestión de recursos, facilitar la comunicación con los clientes y proveedores, y reducir costos en procesos administrativos.

Zurdo y González también destaca la importancia de la formación y capacitación en competencias digitales para que las organizaciones de economía social puedan aprovechar al máximo los beneficios de la digitalización. Asimismo, se enfatiza la necesidad de políticas públicas que fomenten la digitalización en la economía social. Por otro lado, autores como Mazzochi y otros [14] averiguan sobre la recepción de la IA en cuanto a una de sus técnicas el "enfoque de regresión" para analizar la influencia de factores territoriales en la creación y el éxito de los bio-distritos, identificando las características territoriales que influyen en el desarrollo de estas iniciativas. En esa ocasión la IA sirvió de respaldo para averiguar la relación entre determinados factores territoriales con la creación de bio-distritos.

Igualmente analizan los datos de 15 bio-distritos en Italia y utilizan un modelo de regresión múltiple para evaluar la influencia de factores territoriales en el éxito de estas iniciativas. Los resultados indican que los bio-distritos son más exitosos en áreas con una alta concentración de agricultores, una buena infraestructura de transporte y una elevada proporción de tierra cultivable. Además, el éxito de los bio-distritos se correlaciona positivamente con la presencia de instituciones y organizaciones locales que promueven el desarrollo rural y la agricultura sostenible.

No todos son aspectos positivos alrededor de la IA. Un sector de quienes investigan en esta disciplina, la examinan dentro del componente ético; como lo dan a conocer Garcia-Vigil [15] por ejemplo, asevera que la IA ha avanzado significativamente en las últimas décadas, y ha comenzado a transformar diversas áreas de la sociedad, incluyendo la medicina, la educación, el transporte y el entretenimiento. Sin embargo, a medida que la IA se vuelve más omnipresente, surgen preocupaciones éticas sobre su impacto en la privacidad, la seguridad, la justicia y la igualdad. En un argumento reflexivo, Garcia-Vigil [15] recuerda que la ética se refiere a los valores y principios que deben guiar el desarrollo y la implementación de la IA para asegurar que sea utilizada para beneficio de la humanidad y no para su perjuicio.

Adicionalmente, advierte que la IA está transformando nuestra comprensión de la inteligencia humana, y desafiando la noción tradicional de que la inteligencia es una propiedad exclusivamente humana. El autor sostiene que la inteligencia es un concepto complejo y multifacético que se manifiesta en diferentes formas en humanos y máquinas, y que nuestra comprensión de la inteligencia humana debe evolucionar para incluir las capacidades de la IA. En la actualidad, la IA sigue siendo aplicada por la industria automotriz. La página oficial de Ford cita: "Los robots utilizan sensores de alta tecnología para detectar si se interponen dedos o manos en su camino y se detienen inmediatamente, garantizando la seguridad de los trabajadores humanos". Hoy en día estos robots, también cumplen los conceptos de IA, perciben, "razonan" y resuelven problemas como lo demuestran Aguirre y otros [16].

III. METODOLOGÍA

Este trabajo se realiza teniendo en cuenta el método deductivo que como procedimiento de investigación vamos a utilizar información de otros autores, teniendo presente iniciar desde el razonamiento más general y lógico, basado en leyes o principios. Del análisis de cada referente se extrajeron los conceptos que se adaptaban a lo que se trabaja en las empresas en Colombia en temas de logística y cadenas de suministro.

Por otra parte, se trabajó con la técnica de análisis documental, donde se identificaron un total de 54 documentos que se consultaron en la red nacional de bibliotecas Rafael García Herreros, realizando un análisis de elementos comunes de logística y 10 documentos en ingles que tienen relación con la cadena de suministro y logística empresarial.

Del total de documentos analizados, se logró seleccionar un conjunto de 22 refrentes bibliográficos que apoyan la información y conceptos que tenemos en Colombia en términos de logística empresarial y cadena de suministro.

A. La IA aplicada al campo de la logística: beneficios y recomendaciones

En lo que respecta al campo de la logística los estudios examinados reconocen profundos beneficios de la IA, autores como Castán Farrero y otros [17] sugieren que esta tecnología IA ha sido utilizada en diferentes áreas de la gestión de la cadena de suministro, incluyendo la planificación y programación, la gestión de inventarios, el transporte y la logística inversa. Los autores encontraron que la IA está siendo utilizada cada vez más en la gestión de la cadena de suministro y la logística, y que se ha demostrado que

es eficaz para mejorar la eficiencia, reducir los costos y mejorar la satisfacción del cliente. Además, el trabajo de los recién citados proporciona una visión general de los diferentes tipos de técnicas de IA utilizadas en la gestión de la cadena de suministro, como el aprendizaje automático, la lógica difusa y la minería de datos.

Un elemento de relieve de la IA es su capacidad de elaborar tareas complejas sirviéndose de la big data; Zhan y Huang [18] analizan el impacto del análisis de grandes datos en el rendimiento de la cadena de suministro en China. Los autores realizaron varias encuestas a las empresas chinas que utilizan análisis de grandes datos en su cadena de suministro y evaluaron su impacto en términos de eficiencia, flexibilidad y capacidad de respuesta. Los resultados mostraron que el análisis de grandes datos tiene un impacto positivo en la eficiencia y la capacidad de respuesta de la cadena de suministro, pero no en la flexibilidad. Además, los autores sugieren que la implementación efectiva del análisis de grandes datos depende de la disponibilidad de datos precisos y la capacidad de la organización para analizarlos adecuadamente. En esa misma dirección se ubica la investigación de Samuel y otros [19] quienes revelan las diferentes técnicas y herramientas utilizadas para el análisis de grandes volúmenes de datos en el contexto de la cadena de suministro.

En ese marco de medidas disruptivas amparadas en la IA, se puede mencionar a la industria 4.0, que viene transformando la gestión de la cadena de suministro hacia un enfoque más sostenible como lo afirman Ahmed y Abbasi [20]. La literatura consultada advierte que la industria 4.0 puede mejorar la sostenibilidad en diferentes áreas de la gestión de la cadena de suministro, como la planificación, la ejecución y el monitoreo indicados por Ahmed y Abbasi [20]. Estos investigadores encontraron que la industria 4.0 puede mejorar la sostenibilidad de la cadena de suministros a través de la digitalización, la automatización y la conectividad, lo que permite una mejor toma de decisiones y una mayor eficiencia en el uso de recursos. Además, el autor destaca una visión general de las tecnologías clave de la industria 4.0, como el Internet de las cosas (IoT), la inteligencia artificial (IA) y la robótica, y cómo se aplican en la gestión de la cadena de suministro.

Ahora bien, incursionando en investigaciones de autores latinos como Giraldo y otros [3] quienes ofrecen un examen sobre la aplicación la IA en diferentes áreas de la logística, como la gestión de la cadena de suministro, el transporte, la gestión de inventarios y la planificación. Los autores analizan una amplia gama de publicaciones, incluidos artículos de revistas, conferencias y libros, para identificar las tendencias y los avances en la investigación sobre IA y logística. En general, los autores encuentran que la IA se está utilizando cada vez más en la logística, y que las áreas en las que se está aplicando incluyen la toma de decisiones, la predicción de la demanda, el rastreo y seguimiento de los envíos, y la optimización de la cadena de suministro. Los autores también discuten las oportunidades y desafíos que plantea la IA en la logística, como la necesidad de mejorar la calidad de los datos y la transparencia en los algoritmos utilizados.

Años antes los autores citados habían estudiado la aplicación de un modelo de simulación híbrido de una cadena logística simple utilizando tecnología GIS (Sistemas de Información Geográfica). Dicho modelo permitió simular diferentes escenarios y evaluar su efectividad en términos de costos, tiempos de entrega, niveles de inventario, y otros indicadores relevantes. Además, el uso de tecnología GIS permitió una visualización espacial de los diferentes componentes de la cadena logística, lo que facilitó la identificación de cuellos de botella y la toma de decisiones, así lo manifiestan Giraldo y otros [3]. El modelo se basa en una cadena logística simple que consta de cuatro componentes principales: proveedores, centro de distribución, minoristas y clientes. Se presentan tres escenarios diferentes para demostrar la capacidad del modelo para evaluar diferentes estrategias logísticas: un escenario básico, un escenario con un centro de distribución adicional y un escenario con un cambio en la ubicación del centro de distribución. Adicionalmente, los resultados de la simulación indicaron que el modelo puede ser utilizado para optimizar diferentes aspectos de la cadena logística. Los autores concluyeron que la combinación de tecnología GIS y herramientas de simulación puede mejorar significativamente la eficiencia de la cadena logística y reducir los costos asociados con ella así lo demuestra en su análisis de Modelo de simulación hibrido de una cadena logística simple empleando tecnología GIS de Giraldo y otros [3].

En la figura 2 se observa la relación que se da en una cadena de suministro y su red logística, donde se establece una relación entre el cliente y los proveedores, teniendo presente que todos los elementos que están ligados a la logística son importantes y que cumplen un papel importante en este proceso. La producción como proceso de cambio de la materia prima, los diferentes tipos de almacenes donde los productos en sus diferentes acciones (terminado, rechazado, en cuarentena, etc) presentan características propias y diferentes en esta cadena de suministro. Los puntos de ventas que son la conexión que hay entre el producto y el consumidor final el cliente, donde se cumple una función importante desde lo visual, auditivo y en fin de los sentidos humanos como percepción de lo agradable y punto de aceptación que va a tener ese producto o servicio en el cliente.

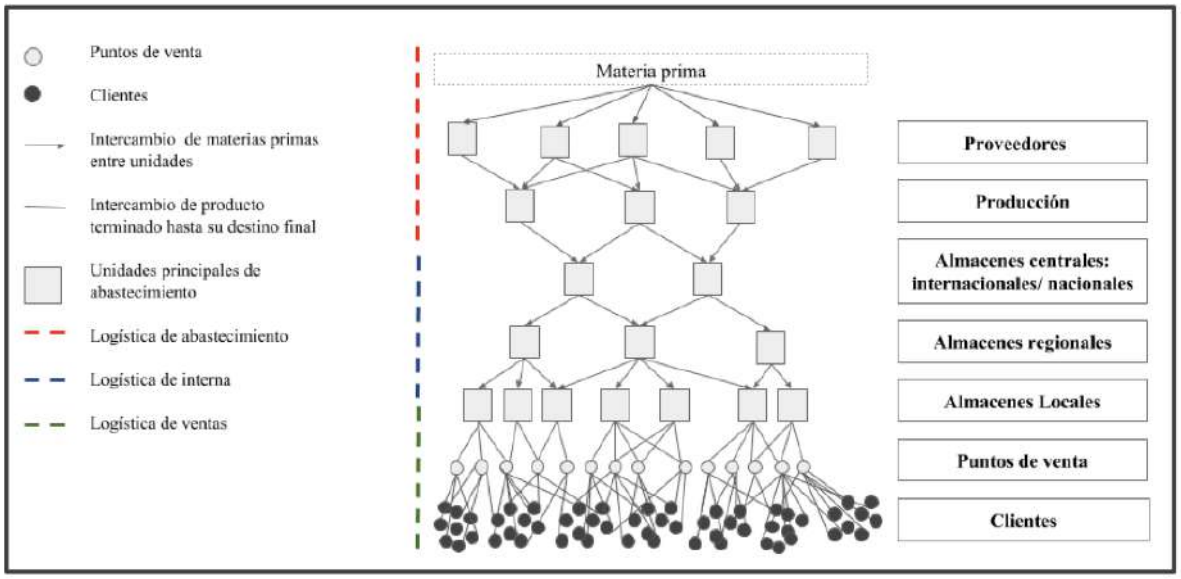

Fig. 2. Representación de una cadena de suministro y su red logística.

Este esquema gráfico define muy bien cuáles son las fases que conforman una cadena de suministro al completo con todos los agentes relevantes que participan en su red logística. Como veníamos diciendo, primero tenemos la logística de entrada o abastecimiento donde se obtienen las materias primas y se inicia el proceso de producción. Después, tenemos la logística interna o de salida que hace referencia al almacenamiento del stock y el abastecimiento a los puntos de venta. Por último, podemos incluir lo que llamaríamos como logística de ventas, que corresponde a la fase final en la que el cliente obtiene el producto así es afirmado por Azcona [21].

De esta manera se puede afirmar que el modelo de simulación híbrido de una cadena logística simple utilizando tecnología GIS, presentado en el trabajo de Giraldo y otros [3] demuestra cómo la combinación de herramientas de simulación discreta y análisis espacial puede mejorar la eficiencia de la cadena logística y reducir los costos asociados con ella. Los resultados de la simulación indicaron que el modelo puede ser utilizado para evaluar diferentes escenarios y estrategias logísticas y para optimizar diferentes aspectos de la cadena logística demostrado por Giraldo y otros [3].

Para finalizar, es axial detenerse en el aspecto ético de la IA aplicado en la logística. Los autores Boudreau y Reynolds [22] desarrollaron un marco ético que puede ser utilizado para evaluar el impacto de la inteligencia artificial en la toma de decisiones logísticas y establecieron algunas recomendaciones para su implementación. En tal sentido, el seguimiento a la buena fe contractual, la evasión de la competencia desleal, y la no sustitución humana del todo tienen especial espacio en sus razonamientos.

Como lo han mencionado varios investigadores, existen beneficios de la IA en logística, como son:

1. *Planificación mejorada de la cadena de suministro*

Las inteligencias artificiales pueden analizar datos de varias fuentes, como datos históricos de ventas, informes meteorológicos y patrones de tráfico, para proporcionar un pronóstico preciso de la demanda. Esta información puede ayudar a las empresas a optimizar sus niveles de inventario, reducir el desperdicio y planificar su cadena de suministro de manera más eficiente.

2. *Optimización de ruta mejorada*

Otra característica de la IA es que puede analizar datos de tráfico en tiempo real, condiciones climáticas y cierres de carreteras para optimizar las rutas de entrega. Esto puede ayudar a las empresas de logística a reducir los tiempos de entrega y el consumo de combustible, lo que se traduce en ahorros de costos.

3. *Mantenimiento predictivo*

Las IA también pueden monitorear equipos y vehículos en tiempo real y predecir cuándo se requiere mantenimiento. Esto puede ayudar a las empresas de logística a programar el mantenimiento de forma proactiva, reduciendo el tiempo de inactividad y evitando averías costosas.

4. *Servicio al cliente mejorado*

Los chatbots impulsados por IA pueden proporcionar a los clientes información en tiempo real sobre sus envíos, tiempos de entrega y otras consultas. Esto puede mejorar la satisfacción del cliente y reducir la carga de trabajo de los equipos de atención al cliente**.**

B. Desafíos de la IA en logística

Si bien hay muchos beneficios de usar IA en la logística, también hay varios desafíos que deben abordarse. Éstas incluyen:

1. *Calidad de los datos*

   Los algoritmos de IA se basan en datos de alta calidad para proporcionar predicciones y recomendaciones precisas. Si los datos son inexactos o están incompletos, el algoritmo puede producir resultados incorrectos.

2. *Costo*

   La implementación de sistemas de inteligencia artificial puede ser costosa y es posible que muchas empresas de logística no tengan el presupuesto para invertir en esta tecnología.

3. *Resistencia al cambio*

   La introducción de nueva tecnología puede ser un desafío y puede haber resistencia por parte de los empleados que no están familiarizados con los sistemas de IA.

IV. RESULTADOS

La consulta de los documentos se realizó por medio de la plataforma de la red nacional de bibliotecas Rafael García Herreros de la corporación UNIMINUTO, que cuenta con una amplia base de consultas, repositorios, bases de datos, libros electrónicos entre otras, que la hace una gran herramienta de consulta y de confiabilidad.

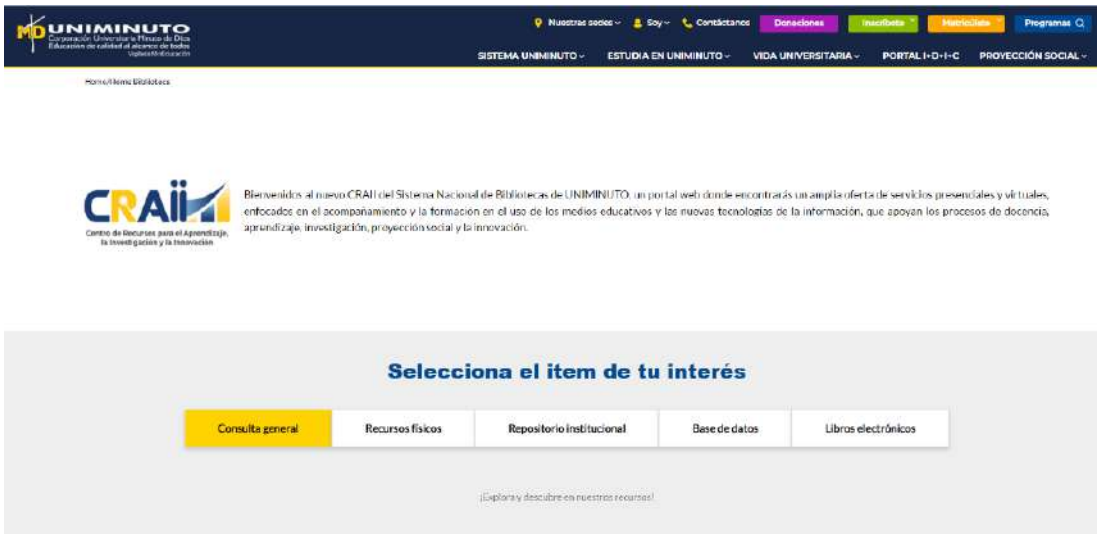

Fig. 3. Imagen representativa del portal de la Biblioteca Rafael Garcia Herreros.

Después de una amplia consulta en el portal de la biblioteca Rafael Garcia Herreros se realizó la revisión de un total de 54 referencias entre bases de datos, repositorios y libros electrónicos. Además, se hizo la búsqueda por temas de interés relacionados con el tema de logística y cadena de suministro empresarial, teniendo en cuenta de igual manera la experiencia que se tiene a nivel industrial en estas labores, y consultando con algunas de las empresas donde se realizan las prácticas profesionales de nuestros estudiantes.

Tabla 1. Consultas bibliográficas por temas en la red nacional de Bibliotecas Rafael García Herreros

Títulos	Cantidad consultada	Español	Inglés
IA-Big data	7	4	3
IA Logística	12	11	1
IA cadena de Suministro	8	7	1
IA Modelado y Simulación	5	5	
IA Robótica	5	5	
IA en la Industria	7	4	3
IA y Discapacidad	2	2	
IA y Medicina	2	2	
IA y aplicaciones	6	4	2
TOTAL	**54**	**44**	**10**

CONCLUSIONES

Fue basta la literatura investigada que dio cuenta sobre le invaluable vinculación entre la IA y los procesos logísticos. Los logros, avances, y beneficios son incuantificables, y la perspectiva a futuro incierta. Por lo pronto, solo vale destacar el apoyo que las herramientas inteligentes están brindando a las empresas de cara a que sus procesos se surtan con la mayor eficiencia y optimización de los recursos de capital y de tiempo, todo lo cual redundará en utilidades para la organización.

La logística es un aspecto esencial de cualquier negocio, y el uso de la tecnología ha facilitado la gestión y optimización de estos procesos. Sin duda, la revisión realizada en este trabajo ha revelado que una de las últimas tecnologías que están revolucionando la industria logística es la inteligencia artificial (IA). La IA tiene el potencial de agilizar el proceso logístico y aumentar la eficiencia, lo que se traduce en ahorros de costos y una mayor satisfacción del cliente.

La IA tiene el potencial de revolucionar la industria de la logística al mejorar la planificación de la cadena de suministro, mejorar la optimización de rutas, permitir el mantenimiento predictivo y mejorar el servicio al cliente. Si bien existen desafíos para implementar sistemas de IA, los beneficios superan con creces los costos. A medida que más empresas adopten la IA en sus operaciones logísticas, la industria se volverá más eficiente y rentable, lo que dará como resultado una mayor satisfacción del cliente y mayores ganancias.

REFERENCIAS

[1] A. Garay Candia, Logistica: conocimientos, habilidades y actitudes, El Cid editor, 2017.
[2] L. A. Mora García, Gestión logística integral: Las mejores prácticas en la cadena de abastecimiento, Eco Ediciones, 2016.
[3] J. Giraldo, O. Castrillon y S. Ruiz, «Modelo de simulación hibrido de una cadena logística simple empleando tecnología GIS,» Revista avances en sistemas e informática, p. 10, 2019.
[4] M. J. Escudero Serrano, Logística de almacenamiento., Paranimfo, 2014.
[5] S. O´Brien y A. Rajabzadeh, The role of artificial intelligence in logistics: A systematic literature review. Transportation research part D, 2020.
[6] O. Alvarez, Inteligencia Artificial y Machine Learning en la Logística, 2022.
[7] M. González García, J. López Cerezo y J. Luján López, «Ciencia, tecnología y sociedad: una introducción al estudio social de la ciencia y la tecnología,» Revista Bibliográfica de Geografía y Ciencias Sociales, p. 324, 2021.
[8] J. C. Ponce Gallegos, A. Torres Soto, F. Quezada Aguilera, A. Silva Sprock, E. Martinez Flor, A. Casali, E. Scheihing, Y. Túpac Valdivia, M. D. Torres Soto, F. Ornelas Zapata, J. Hernández, C. Zavala, N. Vakhnia y O. Pedreño, Inteligencia Artificial, Proyecto Latin, 2014.
[9] F. Herrera Triguero, M. Parras Rosa, J. L. Hidalgo García, S. García, L. Moral y C. Araujo, Inteligencia Artificial, Inteligencia Coimputacional y Big Data, Universidad de Jaén, 2014.
[10] J. Cardenes Doctor, La aplicación de Big Data e Inteligencia Artificial en logística y transporte para la optimización de procesos en empresas, Universidad Pontificia Madrid España, 2022.
[11] O. Bedoya, J. Agudelo y S. Guarin Aristizábal, «Aplicación de técnicas de inteligencia artificial para la detección de tuberculosis pulmonar en Colombia,» Revista EIA, vol. 20, p. 30, 2023.
[12] G. Minetti, C. Salto, H. Alfonso, C. Bermúdez, J. Dielscheider y J. Vargas, «Optimización de la logística de distribución utilizando técnicas de la Inteligencia Artificial,» XXIV Edición del Workshop de investigadores en Ciencias de la Computación, p. 5, 2022.
[13] R. J. Palomo Zurdo y M. González Sánchez, «Un contraste de la divergencia en el modelo de modelo de negocio de las entidades financieras de economía social,» REVESCO. Revista de estudios cooperativos, nº 83, pp. 85-114, 2004.
[14] C. Mazzocchi, C. Bergamelli, A. Sturla y L. Orsi, «Bio-districts and the territory: evidence from a regression approach,» Aestimum, nº 79, pp. 5-23, 2022.
[15] J. García-Vigil, «Reflexiones en torno a la ética, la inteligencia humana,» Gaceta Médica de México, nº 157, pp. 311-314, 2021.
[16] J. Aguirre, F. García, C. Ramírez, S. Floreano y T. Guarda, «Aplicación de la inteligencia artificial en la industria automotriz,» Revista Ibérica De Sistemas e Tecnologias De Informação, nº 42, pp. 149-158, 2021.
[17] J. M. Castán Farrero, J. López Parada y A. Núñez Carballosa, La logística en la empresa: Un área estratégica para alcanzar ventajas competitivas, Ediciones Piramide, 2012.

[18] H.-q. Zhang, L y X.-q. Huang, «The influence of big data analytics on supply chain performance: Evidence from China.,» Journal of Business Research, nº 122, pp. 704-714, 2021.
[19] F. W. Samuel, M. Queiroz, L. Wu y U. Sivarajah , «Big data analytics-enabled sensing capability and organizational outcomes: assessing the mediating effects of business analytics culture,» Annals of Operations Research, 2020.
[20] N. Ahmed y M. S. Abbasi, «Industry 4.0 and sustainable supply chain management: A comprehensive review,» Journal of Cleaner Production, nº 278, 2021.
[21] A. Azcona Puig, La Innovación Tecnológica en Logística. Análisis de Mejores Prácticas y su aplicación al caso de El Corte Inglés., Universidad Pontifica Comillas., 2019.
[22] T. Boudreau y M. Reynolds, «Developing an ethical framework for artificial intelligence in logistics,» Transportation Journal, nº 59, pp. 372-400, 2020.

$$(x+a)^n = \sum_{k=0}^{n} \binom{n}{k} x^k a^{n-k}$$

$$(1+x)^n = 1 + \frac{nx}{1!} + \frac{n(n-1)x^2}{2!} + \cdots$$

Published by:

AutanaBooks
Engineering & Sciences